AD-A147 298

AD

B
R
L

TECHNICAL REPORT BRL-TR-2588

CHARACTERIZATION OF JET-CONTAMINANT INTERACTION FLOW IN CHEMICAL DECONTAMINATION

Lang-Mann Chang

September 1984

DTIC
ELECTE
NOV 2 1984
S
A

APPROVED FOR PUBLIC RELEASE; DISTRIBUTION UNLIMITED.

US ARMY BALLISTIC RESEARCH LABORATORY
ABERDEEN PROVING GROUND, MARYLAND

DTIC FILE COPY

84 10 29 018

Destroy this report when it is no longer needed.
Do not return it to the originator.

Additional copies of this report may be obtained from the National Technical Information Service, U. S. Department of Commerce, Springfield, Virginia 22161.

The findings in this report are not to be construed as an official Department of the Army position, unless so designated by other authorized documents.

The use of trade names or manufacturers' names in this report does not constitute indorsement of any commercial product.

UNCLASSIFIED

SECURITY CLASSIFICATION OF THIS PAGE (When Data Entered)

REPORT DOCUMENTATION PAGE		READ INSTRUCTIONS BEFORE COMPLETING FORM
1. REPORT NUMBER TECHNICAL REPORT BRL-TR-2588	2. GOVT ACCESSION NO. AD-A147 358	3. RECIPIENT'S CATALOG NUMBER
4. TITLE (and Subtitle) Characterization of Jet-Contaminant Interaction Flow in Chemical Decontamination		5. TYPE OF REPORT & PERIOD COVERED Technical Report 6. PERFORMING ORG. REPORT NUMBER
7. AUTHOR(s) Lang-Mann Chang		8. CONTRACT OR GRANT NUMBER(s)
9. PERFORMING ORGANIZATION NAME AND ADDRESS US Army Ballistic Research Laboratory ATTN: AMXBR-IBD Aberdeen Proving Ground, MD 21005-5066		10. PROGRAM ELEMENT, PROJECT, TASK AREA & WORK UNIT NUMBERS 1L161102A71A
11. CONTROLLING OFFICE NAME AND ADDRESS US Army Ballistic Research Laboratory ATTN: AMXBR-OD-ST Aberdeen Proving Ground, MD 21005-5066		12. REPORT DATE September 1984 13. NUMBER OF PAGES 74
14. MONITORING AGENCY NAME & ADDRESS(if different from Controlling Office)		15. SECURITY CLASS. (of this report) Unclassified 15a. DECLASSIFICATION/DOWNGRADING SCHEDULE

16. DISTRIBUTION STATEMENT (of this Report)

Approved for public release; distribution unlimited.

17. DISTRIBUTION STATEMENT (of the abstract entered in Block 20, if different from Report)

18. SUPPLEMENTARY NOTES

19. KEY WORDS (Continue on reverse side if necessary and identify by block number)

Chemical Decontamination	Two-Fluid Flow
Contaminant Droplet	Jet-Droplet Interaction
Water Jet Impingement	Numerical Simulation
One-Fluid Flow	Droplet Movement

20. ABSTRACT (Continue on reverse side if necessary and identify by block number) slp

A numerical simulation and study are presented for characterization of the flow interaction of a water jet with a chemical contaminant droplet on a plane wall, which occurs in chemical decontamination processes. Two models are developed for this analysis, namely, one-fluid flow and two-fluid flow, both governed by the two-dimensional Navier-Stokes equations. Emphases of the study are on the evolution of the contaminant droplet and the effects of various flow parameters. Computer plots of the movement of the droplet are

DD FORM 1 JAN 73 1473 EDITION OF 1 NOV 65 IS OBSOLETE

UNCLASSIFIED

SECURITY CLASSIFICATION OF THIS PAGE (When Data Entered)

20. ABSTRACT (continued)
present. Computed results show that a jet impingement at 45°-60° from the contaminated wall can perform in the most effective and most efficient way in displacing the contaminant. The results also show that an increase in the jet velocity or the cross-sectional area of the jet can greatly improve the cleaning power. However, for a given jet flow rate, it is more advantageous to adopt a jet spray composed of a number of small high-speed jets than one consisting of a single large low-speed jet. The jet-contaminant interactions taking place in confined geometries, such as cavities and corners of two perpendicular walls, are also examined. We have found that an inclined jet is more effective than a normal jet for decontaminating such geometries. In all of the flow cases studied, the impact pressure on the impingement wall far exceeds the steady-state stagnation pressure of the jet.

TABLE OF CONTENTS

Page

LIST OF FIGURES.....5

LIST OF TABLES.....9

I. INTRODUCTION.....11

II. FLOW MODELS.....12

2.1 Two-Fluid Model.....13
2.2 One-Fluid Model.....13

III. FLOW EQUATIONS, METHOD OF SOLUTION AND MESH SETUP.....15

3.1 Flow Equations and Method of Solution.....15
3.2 Mesh Setup.....17

3.2.1 Two-Fluid Flow.....17
3.2.2 One-Fluid Flow.....18

IV. TEST RUN OF COMPUTER CODE AND CONSIDERATIONS OF SURFACE TENSION AND CONTACT ANGLE.....18

4.1 Test Run of the SOLA-VOF Code.....18
4.2 Surface Tension.....19
4.3 Contact Angle.....20

V. COMPUTATIONAL RESULTS.....23

5.1 Two-Fluid Model.....24

5.1.1 Flow Patterns and Viscosity Effects.....24
5.1.2 Optimum Angle of Jet Incidence.....28
5.1.3 Effects of Jet Velocity on Jet Performance....33
5.1.4 Effects of Jet Size on Jet Performance.....33
5.1.5 An Effective and Efficient Means to Improve Jet Performance.....35
5.1.6 Pressure Distribution on Impingement Wall.....37

5.2 One-Fluid Flow 37

5.2.1 Flow Patterns and Viscosity Effects.....37
5.2.2 Effects of Jet Velocity and Jet Size on Jet Performance.....43
5.2.3 Pressure Distribution on Impingement Wall.....47

Accession For
GRA&I
TAB
Unannounced
Justification
Distribution/
Availability Codes
Avail and/or
Dist Special
A-1

TABLE OF CONTENTS (Cont'd)

Page

VI. JET-CONTAMINANT INTERACTIONS IN CONFINED GEOMETRIES.....47

6.1 Flow Patterns.....47

6.1.1 Interactions in Cavities.....47
6.1.2 Interactions at Corners of Two Perpendicular Walls.....52

6.2 Pressure Distribution on Bottom Walls of Confined Geometries.....60

VII. GENERAL REMARKS.....60

7.1 Application of Air Jets.....60
7.2 Arrays of Jets.....60
7.3 Justification of Validity of Two-Dimensional Flow Model.....63
7.4 Pulsating Jets.....64
7.5 Simulation of a Moving Jet.....64

VIII. SUMMARY AND CONCLUSIONS.....64

ACKNOWLEDGEMENT.....65

REFERENCES.....67

NOMENCLATURE.....69

DISTRIBUTION LIST.....71

LIST OF FIGURES

Figure		Page
1	Pre-impingement Flow Configurations	13
2	Setup for Two-Fluid Flow Computation	14
3	Setup for One-Fluid Flow Computation	14
4	Free Surface (or Interface) Across a Mesh Cell	16
5	Relation Between Mesh Size and Displacement S of Droplet Upstream Edge	17
6	Setup for a Normal Jet Impingement on a Plane Wall	19
7	Flow Development of a Normal Jet Impinging on a Wall	20
8	Normalized Impact Pressure on Impingement Wall (Normal Jet)	21
9	Comparison of Droplet Movement with and without Consideration of Surface Tension	22
10	Flow Patterns (Two-Fluid Flow, V_j=5 m/s, θ =45^o)	25
11	Evolution of Droplets	26
12	Movement of Marker Particles in Droplet - Definition of Displacement S	27
13	Displacement of Droplet Upstream Edge S, vs. Time after Commencement of Jet Flow, t, for Various Angles of Jet Incidence, θ (V_j=10 m/s)	29
14	Displacement of Droplet Upstream Edge, S, vs. Time after Commencement of Jet Flow, t, for Various Angles of Jet Incidence, θ (V_j=5 m/s)	29
15	Mean Velocity of Droplet Upstream Edge, S, vs. Time after Commencement of Jet Flow, t, for Various Angles of Jet Incidence, θ (V_j=10 m/s)	30
16	Mean Velocity of Droplet Upstream Edge, S, vs. Time after Commencement of Jet Flow, t, for Various Angles of Jet Incidence, θ (V_j=5 m/s)	31

LIST OF FIGURES (Con'd)

Figure **Page**

17 Displacement of Droplet Upstream Edge, S, vs. Time after Commencement of Jet Flow, t (Water Layer Thickness Increased from 0.2 mm to 0.6 mm).....32

18 Nominal Area Cleaned Per Unit Volume of Jet Fluid Consumed, A/V*, for Various Angles of Jet Incidence, θ 34

19 Displacement of Droplet Upstream Edge, S, vs. Time after Commencement of Jet Flow, t, for Various Jet Velocities, V_j.....35

20 Nominal Area Cleaned Per Unit Volume of Jet Fluid Consumed, A/V*, for Various Jet Flow Rates, Q.....36

21 Flow Developing from an Insufficient Jet Size.....36

22 Displacement of Droplet Upstream Edge, S, vs. Time after Commencement of Jet Flow, t, for Various Jet Sizes, D_j.....38

23 Displacement of Droplet Upstream Edge, S, vs. Time after Commencement of Jet Flow, t, for Various Combinations of Jet Velocity, V_j, and Jet Size, D_j..38

24 Mean Velocity of Droplet Upstream Edge, S, vs. Time after Commencement of Jet Flow, t, for Various Combiunations of Jet Velocity, V_j, and Jet Size, D_j.39

25 Pressure Distributions on Impingement Wall.....40

26 Flow Patterns (Two-Fluid Flow, Thickness of Water Layer above Droplet =0.2 mm, ν_c = 98 mm^2/s, V_j=10 m/s, θ =45°).....40

27 Flow Patterns (Two-Fluid Flow, Thickness of Water Layer above Droplet =1 mm, ν_c = 98 mm^2/s, V_j=10 m/s θ =45°).....41

28 Flow Development (One-Fluid Flow, V_j=10 m/s, ν_w = ν_c =9.8 mm^2/s, θ = 45°).....41

LIST OF FIGURES (Cont'd)

Figure		Page
29	Evolution of Droplets Corresponding to Various Viscosities (One-Fluid Flow, $\theta = 45^{\circ}$)	43
30	Displacement of Droplet Upstream Edge, S, vs. Time after Commencement of Jet Flow, t, (One-Fluid Flow)	44
31	Displacement of Droplet Upstream Edge, S, vs. Time, t, and Mean Velocity, S vs. S	44
32	Displacement S and Mean Velocity S of Droplet Upstream Edge vs. Time After Displacement S Takes Place	45
33	Comparison of Flow Developments Between Two Jet Sizes, D_j = D and 2.5D (One-Fluid Flow, $\nu_w = \nu_c$ = 9.8 mm /s, V_j=10 m/s, θ = 0°, D = 0.6 mm)	46
34	Evolution of Droplets Corresponding to Figure 32	48
35	Pressure Distributions on Impingement Wall	48
36	Pre-impingement Flow Configurations in Cavities	49
37	Pre-impingement Flow Configurations at Corners of Two Perpendicular Walls	49
38a	Flow Developments Corresponding to Figure 36a	50
38b	Evolution of Droplets Corresponding to Figure 38a	51
39a	Flow Developments Corresponding to Figure 36b	52
39b	Evolution of Droplets Corresponding to Figure 39a	53
40a	Flow Developments Corresponding to Figure 36c	54
40b	Evolution of Droplets Corresponding to Figure 40a	55
41	Flow Developments Corresponding to Figure 36d	56
42a	Flow Developments Corresponding to Figure 37a	57
42b	Evolution of Droplets Corresponding to Figure 42a	58

LIST OF FIGURES (Cont'd)

Figure		Page
43	Flow Developments Corresponding to Figure 37b	59
44	Pressure Distributions on Bottom Wall Resulting from Impingement of Figure 36a	61
45	Pressure Distributions on Bottom Wall Resulting from Imingement of Figure 36d	61
46	Pressure Distributions on Bottom Wall Resulting from Impingement of Figure 37a	62
47	Pressure Distributions on Bottom Wall Resulting from Impingement of Figure 37b	62
48	Arrays of Jets	63

LIST OF TABLES

Table **Page**

1 Displacement S (mm) of Droplet Upstream Edge vs. Time after Commencement of Jet Flow for Cases with and without Considerations of Surface Tension and for Different Contact Angles.....19

2 Displacement S (mm) and Mean Velocity S (m/s) of Droplet Upstream Edge vs. Time after Commencement of Jet Flow for Real and Ficticious Viscosities of Jet Fluid, ν_w 42

I. INTRODUCTION

Of various methods proposed for the removal of a chemical contaminant from surfaces of vehicles or other equipment of Army's interest, utilization of liquid jet spray is the most practical and effective one at the current level of technological development. It uses the force produced by the turning of jet stream at the impingement to displace the contaminant. The surfaces then can be decontaminated by moving the jet stream toward the contaminant.

The chemical contaminant is deployed on the surfaces in the form of droplets with a number density of approximately 420 droplets/m^2. Each droplet has a diameter of 2 to 4 mm. The density of the contaminant is very close to that of water, however, its viscosity can be from 10 to 1000 times higher than water viscosity, depending on the enviromental condition.

A high-performance jet spray for decontamination should possess the following two features: a high cleaning speed and an efficient use of jet fluid. These features are particularly important when the jet system is operated in the field where it is often required to decontaminate a surface area in the shortest period of time and with the least consumption of jet fluid. In designing such a system, knowledge of fundamental characteristics of the flow interaction, such as the evolution of the contaminant droplet and the effects of various flow parameters on the flow, is vital. This information can be sought via experiments, but that would require very sophisticated instrumentation and would be very costly. As an alternative, one may use computer simulations based on appropriate flow models. This method can have a much greater flexibility than experiments for examining areas of importance in the flow field and, therefore, can provide better insights into the flow phenomena.

The interaction flow involves two prime fluids, the jet fluid (water) and the contaminant, separated by interfaces. They also may have free sufaces with the ambient (air). The problem is further complicated by the fact that the flow is three-dimensional and is highly transient. Most of the investigations undertaken in the past in jet impingements relate to the VTOL program (vertical takeoff and landing aircraft) or rockect exhaust flows, and they are concerned with jet impingements on a solid plane.[1-4]

---

[1] *G. I. Taylor, "Oblique Impact of a Jet on a Plane Surface," Phil. Trans, R. Soc. A, 260, 1966, pp. 96-100.*

[2] *J. H. Michell, Phil. Trans. A, 181, 1890, pp. 389-431.*

[3] *A. Rubell, "Computations of Jet Impingement on a Flat Surface," AIAA J., 18, No. 2, February 1980, pp. 168-175.*

[4] *A. Rubell, "Computations of the Oblique Impingement of Round Jets upon a Plane Wall," AIAA J., 19, No. 7, July 1981, pp. 863-871.*

Steady two-dimensional jet impingements on a liquid surface were considered by Hunt[5] and Vanden-Broeck.[6] They characterized the wave-like hydrodynamic instability that occurs at the interface of a gas jet and a liquid surface by using simplified theories, but made no predictions of the movement of the liquid and the pressure distribution in the flow field, which are of interest to us.

In this study we focus our attention on the interaction of a water jet with a single contaminant droplet. We simplify the problem by treating it as a two-dimensional flow. Two models, called one-fluid flow and two-fluid flow, were developed to treat two pre-impingement configurations: present and absent water coverage over the droplet. The flow field is governed by the unsteady Navier-Stokes equations which were solved numerically via finite difference schemes using the SOLA-VOF code.[7] We implemented a viscosity relation in the computer code to adapt it to the present case with two fluids having distinct viscosities.

The purpose of the present study is to characterize the jet-contaminant interaction and to provide useful data for design of the jet spray. Results presented in this report consist of computer-generated flow patterns which show the flow development, effects of various parameters on the flow, and impact pressures on the impingement wall. Also presented are flow developments of jet-contaminant interactions in cavities and at corners of two perpendicular walls.

II. FLOW MODELS

Figure 1 depicts two pre-impingement flow configurations which can occur in decontamination processes. In the first configuration, shown in Figure 1a, a water jet is directed at a contaminant droplet with a water coverage over it on a plane wall. The second configuration, shown in Figure 1b, differs from the first in that there is no initial water coverage over the droplet. In order to characterize the flows developing from these two configurations, we have developed a two-fluid model and a one-fluid model. Both models describe a two-dimensional viscous flow and can be handled by

---

[5] *J. N. Hunt, "Wave Formation in Explosive Welding," Philosophical Magazine, 8th Series, Vol. 17, p. 669-680, 1967.*

[6] *J. M. Vanden-Broeck, "Deformation of a Liquid Surface by an Impingement Gas Jet," SIAM J. Appl. Math., 41, No. 2, October 1981, pp. 306-309.*

[7] *B. D. Nicholas, C. W. Hurt, and R. S. Hotchkiss, "SOLA-VOF: A Solution Algorithm for Transient Fluid Flow with Multiple Free Boundaries," Los Alamos Scientific Laboratory Report No. LA-8355, 1980.*

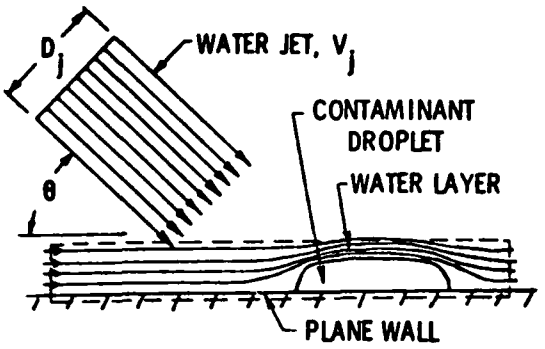

a. Droplet with Water Layer Coverage (Two-Fluid Model)

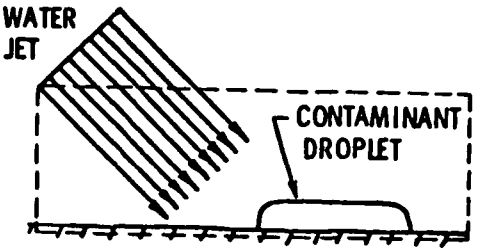

b. Droplet without Water Coverage (One-Fluid Model)

Figure 1. Pre-impingement Flow Configurations

the SOLA-VOF computer code which can handle flow problems involving two immiscible fluids separated by interfaces in a region without voids or flow problems involving one fluid with voids (air).

2.1 Two-Fluid Model

This is a model of a channel-type flow bounded by the dashed line indicated in Figure 1a, covering the major part of the flow region. As shown in Figure 2, the channel contains two fluids (water and contaminant) separated by an interface. The upper wall of the channel coincides with the upper boundary of the water layer so as to eliminate consideration of its free surface with the ambient. An outflow boundary condition is specified at this wall and at the ends of the channel, allowing the fluids to flow out the region. The contaminant which occupies the shaded rectangular region is assumed to perfectly wet the lower wall of the channel. To account for viscous effects, a no-slip condiation is used at this wall. Finally, a steady and uniform jet stream at an angle of incidence, θ , is prescribed along a segment of the upper wall.

2.2 One-Fluid Model

Results of computations with the two-fluid model, given in Section 5-B of this report, show that for a close-in impingement the movement of the contaminant droplet at its early stage is insensitive to the the viscosity of jet fluid. In addition, the density of the contaminant, 1070 kg/m^3, is very close to that of water, 1000 kg/m^3. Therefore, we can simplify the problem by setting the physical properties of the jet fluid (water) equal to that of the contaminant and treat the jet-contaminant interaction as a one-fluid flow problem. Figure 3 depicts the flow region for computation, bounded by the dashed line marked in Figure 1b. In this model, only the

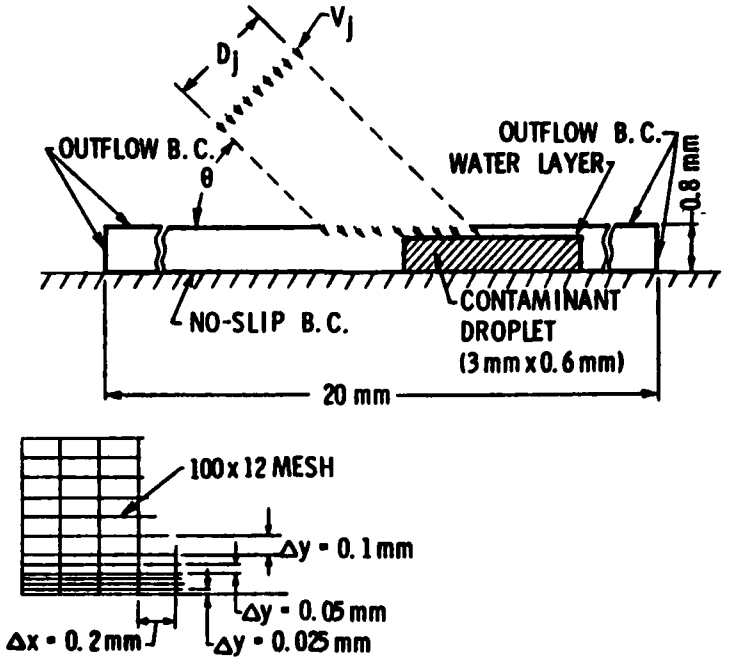

Figure 2. Setup for Two-Fluid Computation

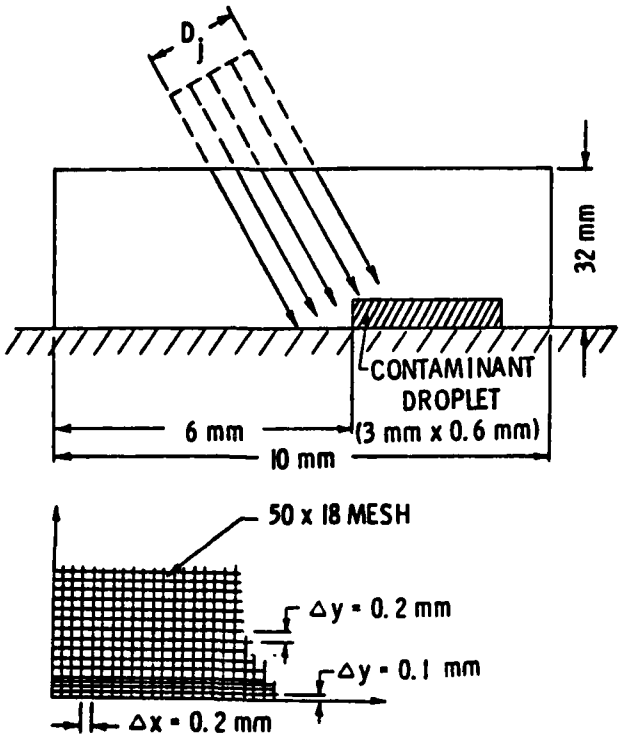

Figure 3. Setup for One-Fluid Flow Computation

free surface with the ambient needs to be traced, but not the water-contaminant interface since both liquids are assumed to be identical. The model is suitable for the treatment of the flow configuration of Figure 1b. The two-fluid model cannot be used for this configuration because it would require the tracing of both the free surface and the interface, and thus would be beyond the capability of the SOLA-VOF code.

III. FLOW EQUATIONS, METHOD OF SOLUTION, AND MESH SETUP

3.1 Flow Equations and Method of Solution

The governing equations of the above two model flows are the continuity equation

$$\frac{1}{\rho c^2}\frac{\partial p}{\partial t} + \frac{\partial u}{\partial x} + \frac{\partial v}{\partial y} = 0 \tag{1}$$

and the momentum equations

$$\frac{\partial u}{\partial t} + u\frac{\partial u}{\partial x} + v\frac{\partial u}{\partial y} = -\frac{1}{\rho}\frac{\partial p}{\partial x} + \nu\left[\frac{\partial^2 u}{\partial x^2} + \frac{\partial^2 u}{\partial y^2}\right] \tag{2}$$

$$\frac{\partial v}{\partial t} + u\frac{\partial v}{\partial x} + v\frac{\partial v}{\partial y} = -\frac{1}{\rho}\frac{\partial p}{\partial y} + \nu\left[\frac{\partial^2 v}{\partial x^2} + \frac{\partial^2 v}{\partial y^2}\right] \tag{3}$$

where t is time u and v are the x-component (along the channel) and the y-component (normal to the channel) of the flow velocity, respectively. The density ρ, the sound speed c, and the kinematic viscosity ν are assumed to be constant. The Reynolds numbers based on the jet thicknesses and the jet velocities used in this study are between 20 and 2000. Within this range, Eqs. (2) and (3) are felt to be appropriate without considering turbulence effects.

In order to track the water-contaminant interface in two-fluid flows or the free surface in one-fluid flows, the SOLA-VOF code uses a "fractional volume of fluid" function F. The function satisfies the following relation

$$\frac{\partial F}{\partial t} + u\frac{\partial F}{\partial x} + v\frac{\partial F}{\partial y} = 0 \tag{4}$$

which states that F moves with the fluid. In two-fluid flows, the value of F in a computational cell is equal to the fractional volume of the cell that is occupied by the first fluid (say, contaminant). A unit value of F

corresponds to a cell full of the first fluid, whereas a zero value indicates that the cell contains only the second fluid (water from the jet and the water layer over the contaminant). Cells with F values between zero and one contain an interface, as illustrated in Figure 4. In one-fluid flows, the second fluid has the meaning of a void and F traces the free surface.

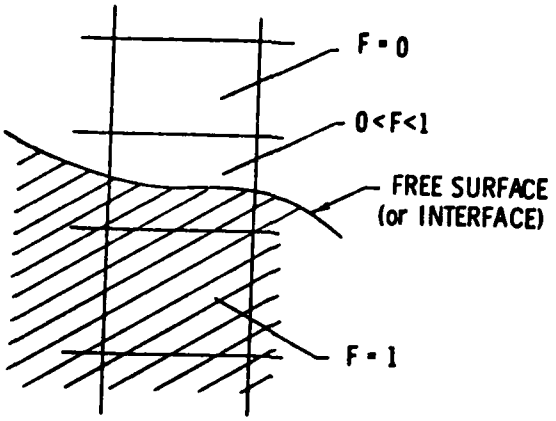

Figure 4. Free Surface (or Interface)
Across a Mesh Cell

The SOLA-VOF Code solves the momentum Eqs. (2) and (3) by using an explicit finite difference scheme and the continuity Eq. (1) by using an implicit finite difference method. The solution of Eq. (4) is obtained by using a Donor-Acceptor flux approximation. Details of the solution method are given in Reference 7. In order to better observe the evolution (location and shape) of the droplet, marker particles were embedded in the region originally covered by the droplet. These particles move with the fluid, but do not affect the flow.

The SOLA-VOF code requires that the viscosities of the two fluids in a two-fluid flow case are equal. To adapt the code to the present problem involving two fluids with distinct viscosities, we used the viscosity relation

$$\nu = \nu_c F + (1-F)\,\nu_w \qquad (5)$$

where ν_c and ν_w are the kinematic viscosities of contaminant and water, respectively, and ν is the average kinematic viscosity of the two fluid mixture in the cell. Similarly, the density in a cell was approximated by

$$\rho = \rho_c F + (1-F)\rho_w \qquad (6)$$

By Eqs. (5) and (6) the values of ν and ρ in a cell are averages weighed by the value of F. For instance, in a cell full of contaminant the value of F is one and thus $\nu = \nu_c$ and $\rho = \rho_c$.

3.2 Mesh Setup

For the numerical computations an Eulerian mesh was used, consisting of rectangular cells of variable sizes with finer zoning near the impingement wall. The use of a variable mesh can substantially save computer costs without sacrificing the accuracy of computation in the regions of main interest.

3.2.1 Two-Fluid Flow. Figure 2 shows part of the 100x12 mesh of the flow region to be analysed. The mesh size in the x-direction is uniform, Δx=0.2 mm, while the mesh size in the y-direction is gradually reduced from Δy=0.1 mm at the top to Δy=0.025 mm (approximately 4% of the droplet height) at the bottom of the flow channel. In order to test the appropriateness of the mesh, computations with slightly finer as well as slightly coarser meshes were performed. The only visible variation noticed was the location of the tip of the upstream edge of the droplet immediately above the wall. This variation is to be expected because, as illustrated in Figure 5, the mesh size near the wall directly affects the calculated magnitude of the displacement S of the droplet upstream edge. This effect will be discussed in Subsection A-1 of Chapter 5.

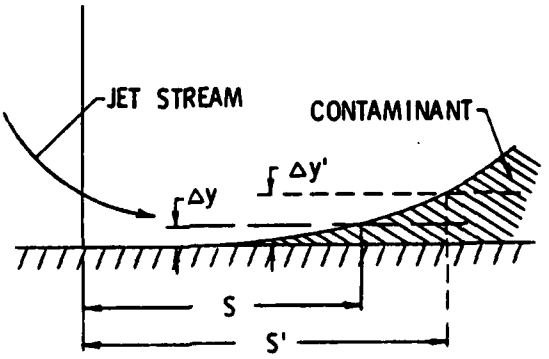

Figure 5. Relation Between Mesh Size and Displacement S of Droplet Upstream Edge

3.2.2 One-Fluid Flow. Figure 3 depicts the computational domain for the one-fluid flow analysis. Initially, a uniform velocity is specified in all mesh cells inside the jet region and the velocity is zero elsewhere. For subsequent time levels, only the mesh cells along the upper boundary of the jet region supply a steady and uniform jet stream.

The lower part of Figure 3 shows a portion of the 50x18 mesh for numerical computation. The mesh size was chosen for the purpose to generate patterns using the one-fluid model. Determination of effects of flow parameters, which requires a higher accuracy, was done by using the two-fluid model.

IV. TEST RUN OF COMPUTER CODE AND CONSIDERATIONS OF SURFACE TENSION AND CONTACT ANGLE

4.1 Test Run of the SOLA-VOF Code

As a test run of the computer code, we calculated the pressure distribution on a plane wall impinged by to a two-dimensional, incompressible, inviscid, normal jet impingement. The result was compared with the steady-state pressure calculated from the following relations given in Tayor's paper:[1]

$$P(x_1) = (1/2)\ \rho\ v_j^2(1 - u_1^2) \tag{7}$$

$$u_1 = (-1 - q\cos\Theta) + \sqrt{(1 - q^2)\sin\Theta} \,/\, (q - \cos\Theta) \tag{8}$$

$$x_1 = (1/2)[(1 + \cos\Theta)\ln(1 + q) - (1 - \cos\Theta)\ln(1 - q)] + \sin\Theta \sin^{-1} q \tag{9}$$

where $u = U/V_j$ (U being the fluid velocity on the wall), $x_1 = \pi\ x/(\text{thickness of jet})$, x is the distance along the wall from the stagnation point, q is an auxiliary variable to be eliminated between Eq. (8) and Eq. (9), and θ is the angle of jet incidence.

Figure 6 is the setup of flow region for the test problem. There is a fluid column initially standing on the plane wall with a uniform flow velocity 100 m/s specified in the fluid region. For subsequent time levels, the uniform flow velocity remains only along the upper boundary of the column, while the lower part of the column deforms continuously until a steady flow is established. Plots in Figure 7 show the flow development generated by the computer. The instantaneous pressure profiles on the impingement wall at times up to 0.4 millisecond (ms) are presented in Figure

8. At time equal to 0.4 ms, the pressure approaches the steady-state valve and the pressure profile is very close to the steady-state pressure profile calculated from Eq. (7).

4.2 Surface Tension

The surface tension at the water-contaminant interface has the magnitude of 1-2 dynes/mm.[8] The effect of the surface tension was tested by computing the displacement S of the droplet upstream edge versus time for a sample flow. The resulting displacements and droplet profiles are given in Table 1 and Figure 9, respectively. There is virtually no difference between results with and without consideration of surface tension. Therefore, in order to save computer time, we neglected the surface tension in subsequent computations.

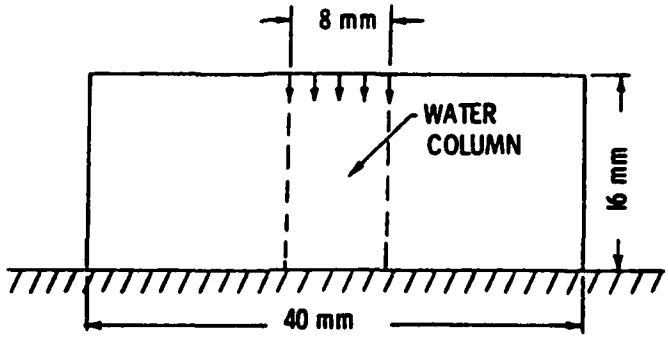

Figure 6. Setup for a Normal Jet Impingement on a Plane Wall

Table 1. Displacement S (mm) of Droplet Upstream Edge vs. Time after Commencement of Jet Flow for Cases with and without Considerations of Surface Tension and for Different Contract Angles

TIME (ms)	SURFACE TENSION		
	0	2 dynes/mm	
	CONT. ANG. = 90°	CONT. ANG. = 45°	CONT. ANG. = 90°
0.04	0.195	0.195	0.195
0.08	0.428	0.427	0.428
0.12	0.673	0.673	0.673
0.16	0.910	0.910	0.910
0.20	1.149	1.147	1.148
0.24	1.369	1.369	1.370
0.28	1.583	1.582	1.583

$V_j = 5$ m/s, $\nu_c = 9.8$ mm^2/s, $\theta = 56.28^0$

[8] *J. Matta, U.S. Army Chemical Research and Development Center (CRDC), private communication, January 1983.*

4.3 Contact Angle

Because the contact angle of the contaminant with the wall surface has not been well documented, it was assumed to be 90° in this study. To test the significance of the angle for the results, we picked another angle of 45° for a sample calculation. Table 1 lists the results in comparison to the 90° case. The sample calculation shows that the contact angle does not influence the results.

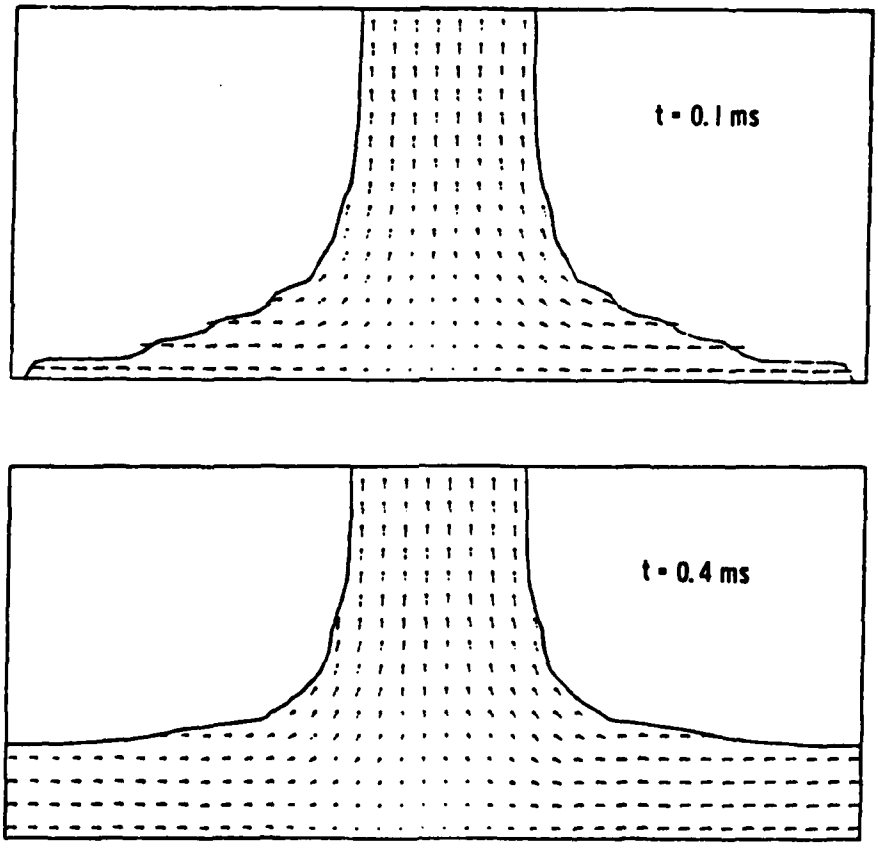

Figure 7. Flow Development of a Normal Jet Impinging on a Wall

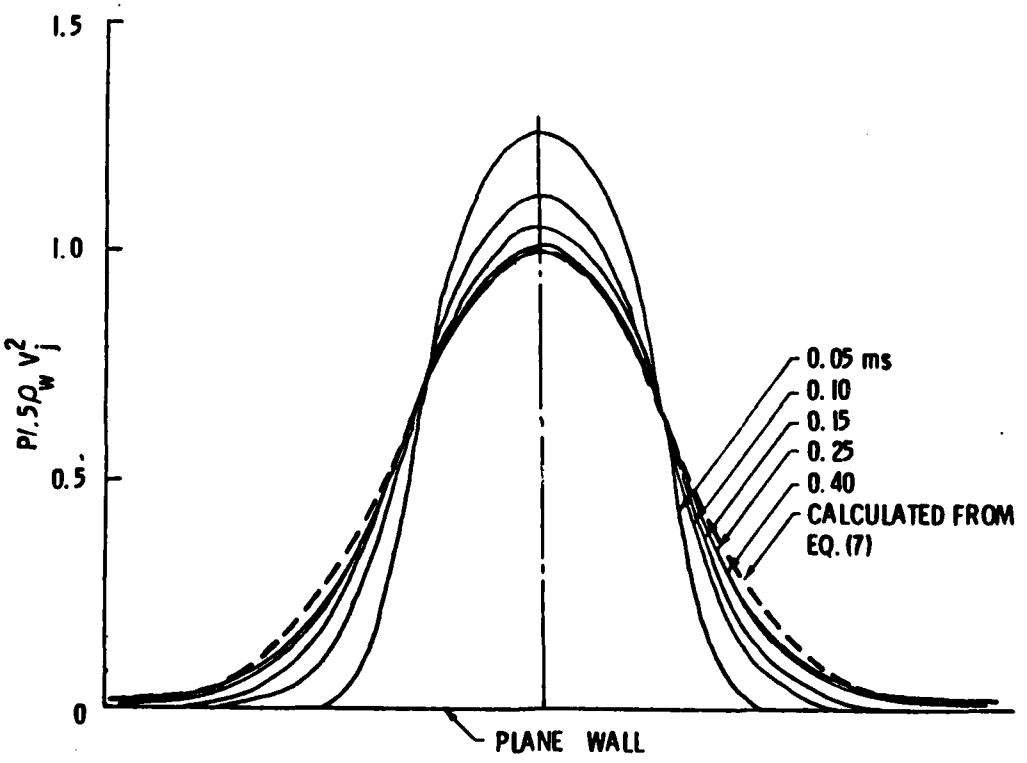

Figure 8. Normalized Impact Pressures on Impingement Wall (Normal Jet)

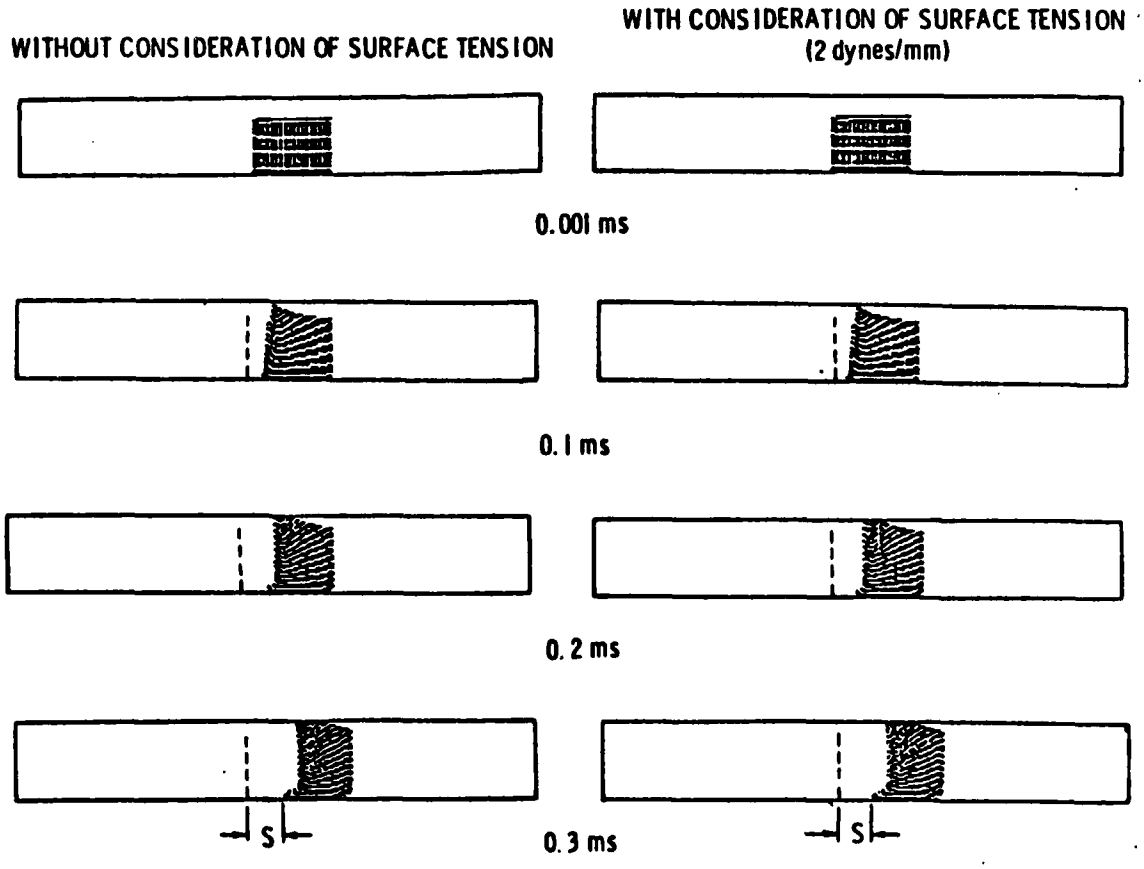

Figure 9. Comparison of Droplet Movements with and without Consideration of Surface Tension

V. COMPUTATIONAL RESULTS

We present results for the following ranges of input data:

θ = angle of jet incidence = 0° - 90°

D_j = jet size (thickness of jet in two-dimensional model)

= 1.83 - 3.66 mm

V_j = jet velocity = 5 - 12.5 m/s, uniform and steady

ρ_w = water density = 1000 kg/m^3

ρ_c = contaminant density = 1070 kg/m^3

ν_w = kinematic viscosity of water = 0.98 mm^2/s

ν_c = kinematic viscosity of contaminant = 9.8 - 980 mm^2/s

Droplet dimensions: 3 mm x 0.6 mm (length by height)

The jet velocities chosen produce stagnation pressures of 12.4 - 75.8 kPa (1.8 - 11 psi), which are practical for decontaminations. The dimensions of the contaminant droplet represent the average droplet size deployed on a plane wall. Our computational results indicate that for such a droplet size the jet thicknesses given above can perform the decontamination effectively and efficiently.

The principal results presented include:

a) flow patterns

b) contaminant viscosity effects

c) optimum angle of jet incidence at which the jet performs best

d) effects of jet velocity and jet size on jet performance

e) improvements of decontaminating speed and efficiency of jet fluid usage

f) pressure distribution on the impingement wall

Some of the results were only obtained by using the two-fluid model which has a higher accuracy. These results are presented in the next section. Results obtained by the one-fluid model will be presented in Section 5-B.

5.1 Two-Fluid Model

5.1.1 Flow Patterns and Viscosity Effects. Figure 10 presents two sets of flow development for times up to 0.2 ms after the start of the jet impingement. They correspond to the two contaminant viscosities ν_c = 9.8 mm^2/s (10 ν_w) and ν_c =980 mm^2/s (1000 ν_w), respectively. The plots have been magnified by a factor of 3 in the vertical direction in order to provide a clear flow visualization near the bottom wall. The arrows in the flow region represent the local fluid velocities. The figures show that the contaminant viscosity has a pronounced effect on the displacement S of the droplet upstream edge as well as on the droplet profile. In the low viscosity case the jet stream toward the droplet is nearly parallel to the bottom wall, whereas in the high viscosity case the jet stream is lifted off the wall. It is interesting to note that as the time progresses, part of the fluid near the downstream edge of the droplet, especially in the high viscosity case, moves toward the bottom wall behind the droplet. Apparently, a low pressure region is created behind the lower portion of the droplet, similar to the flow phenomena that appears behind a stationary obstacle. Figure 11 is a map of the marker particles embedded in the droplet region.

The displacement S indicated in Figure 11 is defined as the distance from the initial location of the upstream edge of the droplet (marked by the dashed line) to the nearest marker particle on the first row above the impingement surface. We embedded 24 rows of marker particles uniformly across the droplet in the vertical direction, and there were 30 marker particles in each row. As illustrated in Figure 12, the nearest marker particle from the dashed line is not always the one which originally resided at the very left end of the first row. This is because the jet stream is lifted off the surface and, as a consequence, the marker particles in the front are carried upward. The location of each marker particle following the jet impingement can be traced and printed out by the computer. The displacement S, as defined, is dependent on the number of rows embedded and on the fineness of the computational grid. A larger number of rows and a finer mesh size would result in a smaller displacement S and theoretically $S \to 0$ as the marker particle approaches the wall. In the present study, the finest cell size in the vertical direction used near the surface was 0.025 mm, which is approximately 4% of the droplet height. The initial distance between the first row of marker particles and the surface was also 0.025 mm. Hence our definition of S is essentially the displacement of contaminant particles that are initially more than 0.025 mm off the wall.

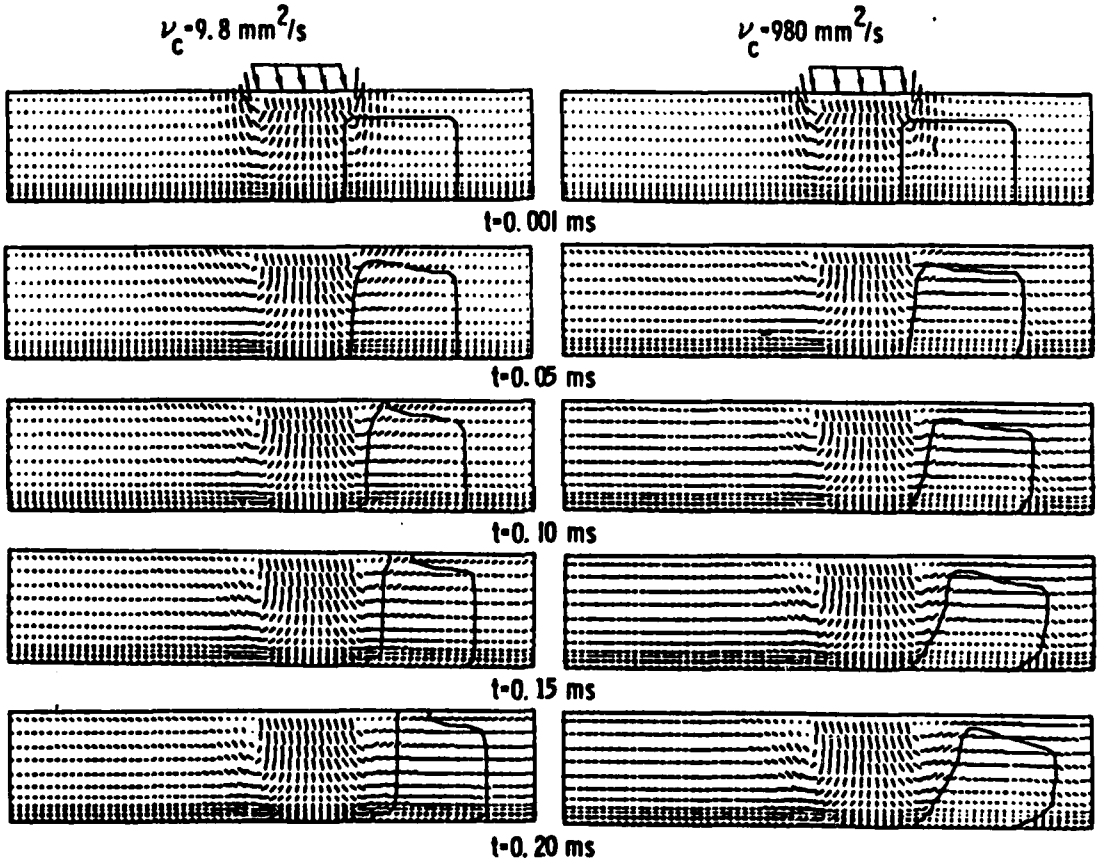

Figure 10. Flow Patterns (Two-Fluid Flow, V_j=5 m/s, θ = 45°)

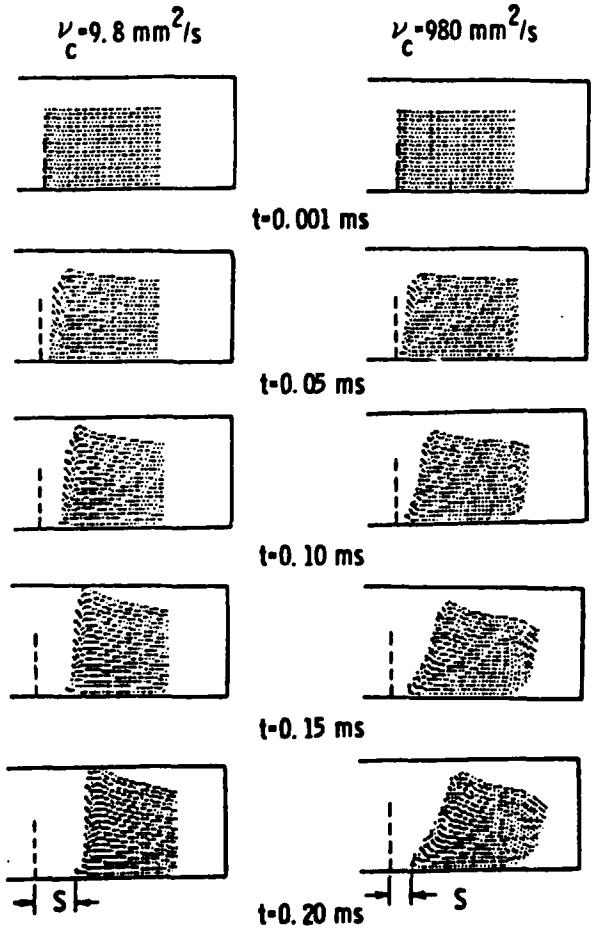

Figure 11. Evolution of Droplets

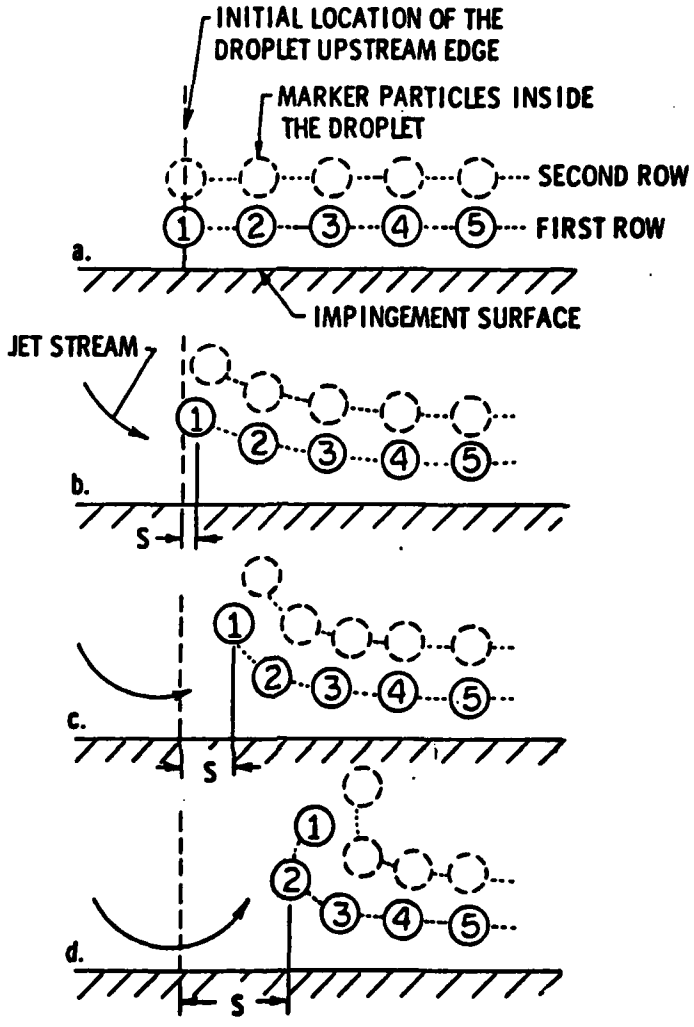

Figure 12. Movement of Marker Particles in Droplet - Definition of Displacement S.

5.1.2 **Optimum Angle of Jet Incidence.** The angle of jet incidence plays a key role in displacing the contaminant. A small angle causes a large fraction of jet stream to move toward the droplet, but a small impingement force on the contaminant near the wall. A large angle, on the other hand, has reverse effects. Therefore, there is an optimum angle at which a jet performs best in removing the contaminant.

Prior to proceeding to optimization of the angle of incidence, we have to note that the performance of the jet spray should be evaluated from two aspects, namely, the cleaning speed and the efficiency of jet fluid usage. The efficiency of jet fluid usage may be important in the areas, especially in the field, where the supply of jet fluid can be limited.

In order to optimize the angle of jet incidence, we used several values between 19.8° and 90° to compute the displacement of the droplet as a function of time following the impingement. At each angle the jet was located such that the impingement takes the shortest time to displace the upstream edge of the droplet a prescribed distance, one third of the original droplet length. A larger prescribed distance likely would not change the results because the movement of the droplet at the very early stage suffices to define the performance of the jet. The angle was optimized by maximizing the cleaning speed and minimizing the expenditure of jet fluid. The particular values of the angle for the computations were chosen to be conveniently adapted to the computational mesh.

Cleaning Speed

The cleaning speed, which is the rate of decontamination, is defined as an average velocity of the movement of the droplet upstream edge along the wall. The average is taken over the time t needed to move the edge by S mm, that is $\dot{S} = S/t$. Figures 13 and 14 show the displacement S of the droplet upstream edge versus time for the jet velocities $V_j = 10$ m/s and $V_j = 5$ m/s, respectively. The dashed lines represent the results for the case that the contaminant viscosity is equal to 10 times water viscosity (i.e., $= 10\ \nu_w$) and the solid lines for $\nu_c = 1000\ \nu_w$. Figures 15 and 16 present the corresponding mean velocities and show that S at a given time t increases with the angle of incidence, θ, until θ reaches 56.28°. Beyond that angle, S decreases except in the case of low jet velocity and extremely large viscosity shown in Figure 16. When the water layer which initially covers the droplet shown in Figure 1a is increased from 0.2 mm, which is used for Figures 13 and 14, to 0.6 mm, the result shown in Figure 17 also indicates that $\theta = 56.28^{\circ}$ results in a better jet performance than any other angle.

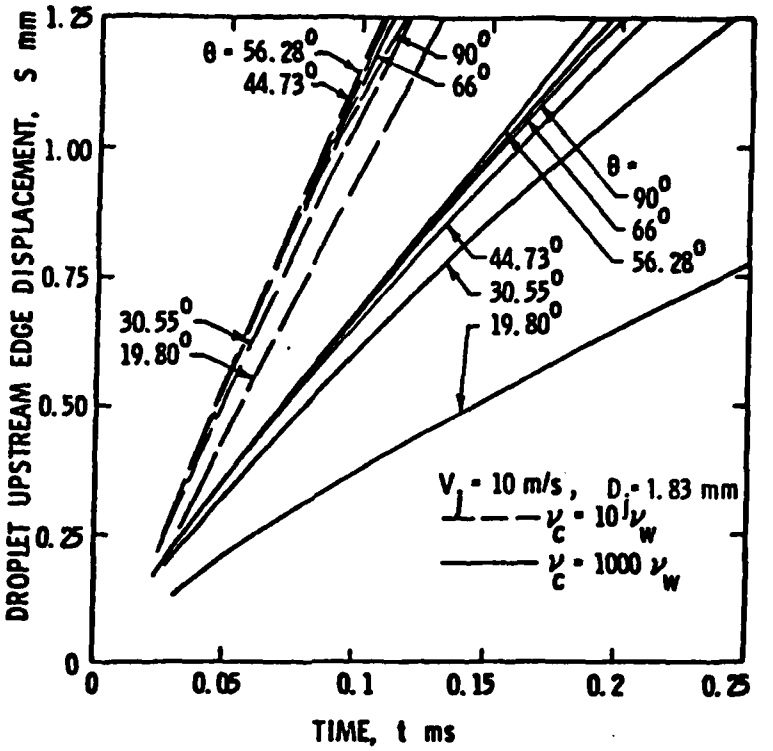

Figure 13. Displacement of Droplet Upstream Edge, S, vs. Time after Commencement of Jet Flow, t, for Various Angles of Jet Incidence, θ (V_j = 10 m/s)

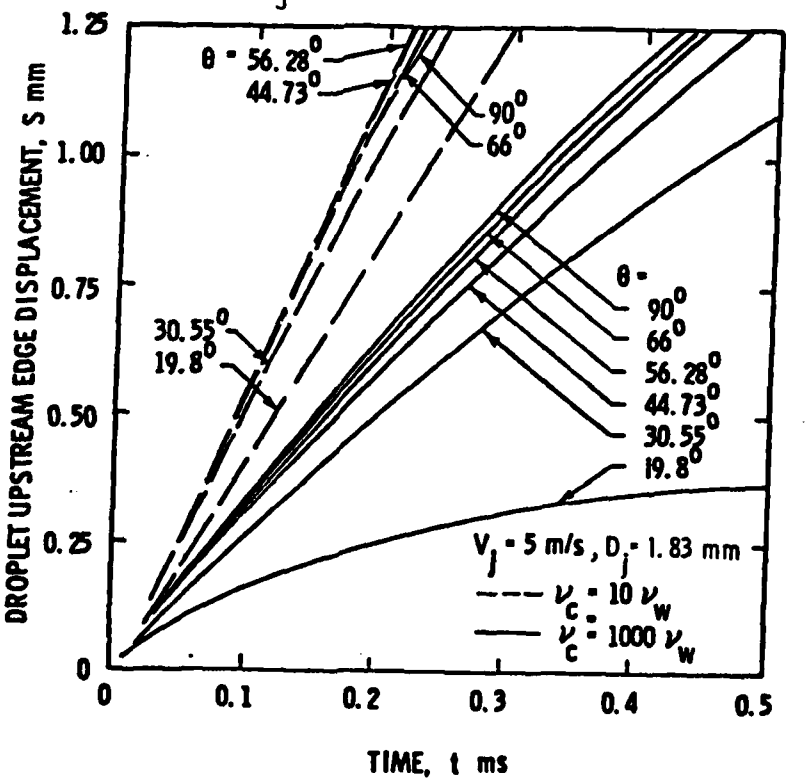

Figure 14. Displacement of Droplet Upstream Edge,S, vs. Time after Commencement of Jet Flow, t, for Various Angles of Jet Incidence, θ (V_j = 5 m/s)

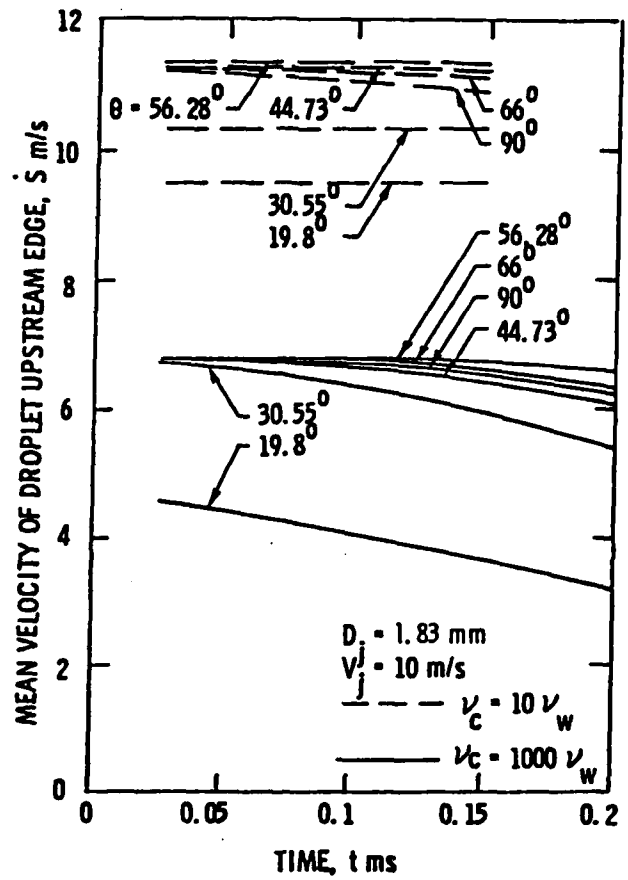

Figure 15. Mean Velocity of Droplet Upstream Edge, $\dot{S}$, vs. Time after Commencement of Jet Flow, t, for Various Angles of Jet Incidence, θ (V_j = 10 m/s)

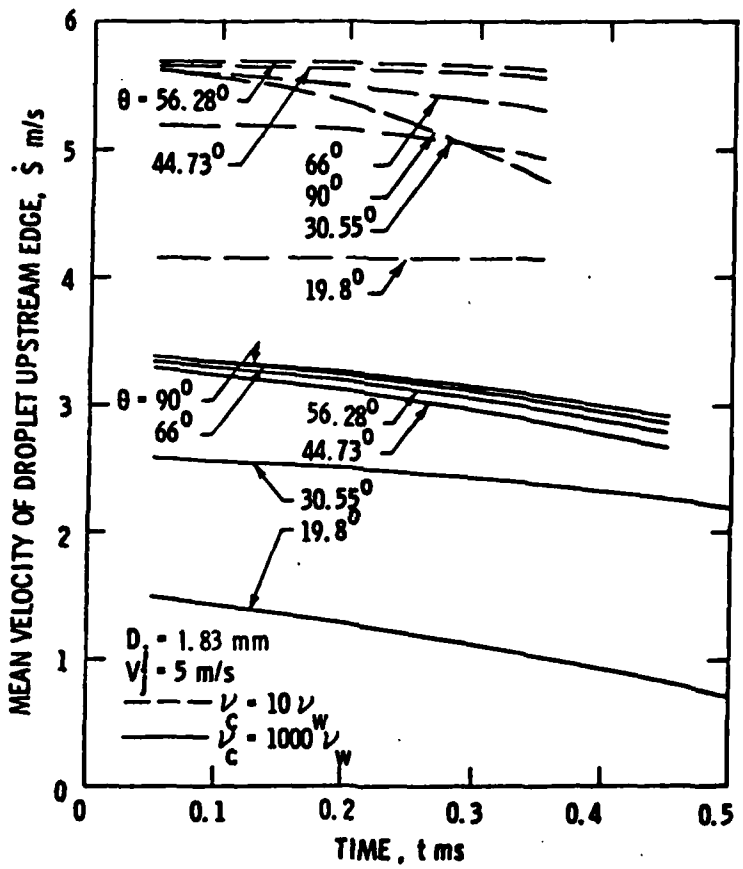

Figure 16. Mean Velocity of Droplet Upstream Edge, S, vs. Time after Commencement of Jet Flow, t, for Various Angles of Jet Incidence, θ(V_j = 5 m/s)

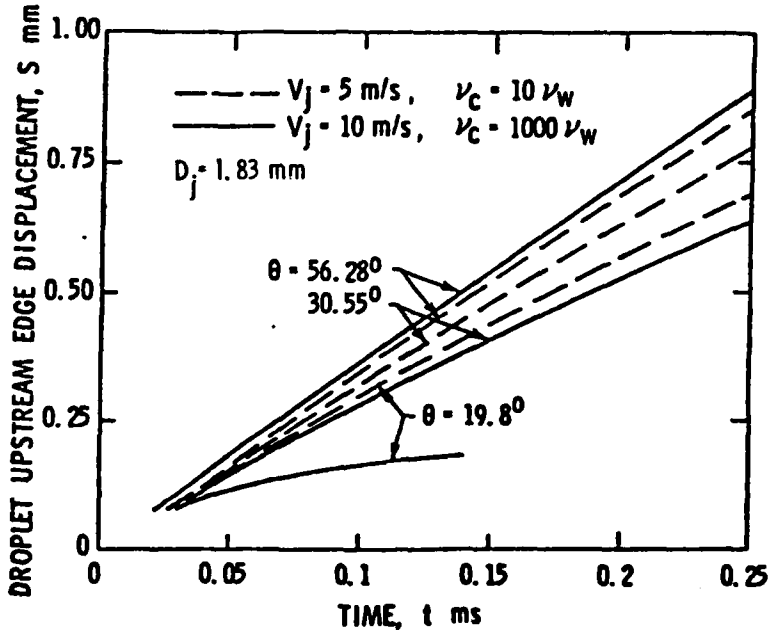

Figure 17. Displacement of Droplet Upstream Edge, S, vs. Time after Commencement of Jet Flow, t (Water Layer Thickness Increased from 0.2 mm to 0.6 mm)

When the contaminant viscosity is extremely large and the jet velocity is low, the normal force is the principal mechanism to break up and displace the droplet. Because the normal force is produced by the turning of flow direction and is proportional to θ, S increases monotonically with θ to 90° in such cases, as shown by the solid curves in Figure 14.

Efficiency of Jet Fluid Usage

In Figure 18, "A" denotes the surface area which has been cleaned (decontaminated) and "V*" the volume of jet fluid consumed for cleaning the area. For a unit width of jet in the present two-dimensional model, we define that $A = S = \dot{S} t$ m^2 and $V^* = V_j D_j t$ m^3. Then A/V*, called the nominal area cleaned per unit volume of jet fluid consumed, indicates how efficiently the jet fluid is used. The curves show that a jet at an angle of incidence between 45^o and 60^o will achieve the most efficient use of jet fluid. They also show that when θ is reduced below 40°, the efficiency falls sharply.

5.1.3 Effects of Jet Velocity on Jet Performance. We expect that the jet velocity affects both the cleaning speed and the efficiency of jet fluid usage. A larger jet velocity produces a greater normal force on the contaminant and, accordingly, more cleaning power, as shown in Figure 19. This result can also be recognized when we compare Figure 16 with Figure 15, in which the cleaning speed has been increased substantially as the jet velocity V_j is raised from 5 m/s to 10 m/s. A larger jet velocity, however, consumes more jet fluid in a given period of time and its impact on the efficiency of jet fluid usage has to be examined.

Figure 20 reveals that the efficiency monotonically increases with the jet velocity in the range studied.

5.1.4 Effects of Jet Size on Jet Performance. In the two-dimensional model, the jet size D_j is simply the thickness of the jet. If D_j is too small, say, less than the height (0.6 mm) of the droplet on a plane wall, the jet stream towards the droplet can not cover the entire leading surface of the droplet and it becomes a jet flow submerged in the droplet as depicted in Figure 21. The cleaning power will certainly be low. Although no extensive computations have been performed in this study to determine the minimum size required for D_j, indications based on the results in various flow cases show that a value larger than one half the droplet length (diameter in three-dimensional cases) is adequate.

Figure 22 reveals that the displacement S at a given time and consequently the cleaning speed increase with jet size D_j. However, the efficiency of jet fluid usage indicated in Figure 20 decreases gradually as D_j is increased in both low and high contaminant viscosity cases.

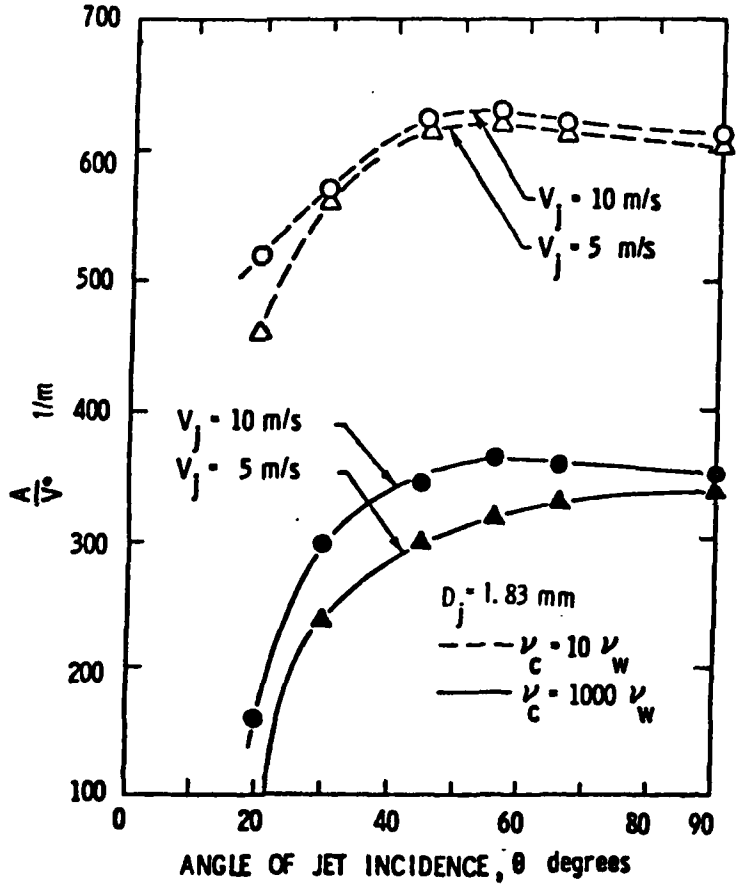

Figure 18. Nominal Area Cleaned Per Unit Volume of Jet Fluid Consumed, A/V^*, for Various Angles of Jet Incidence, θ

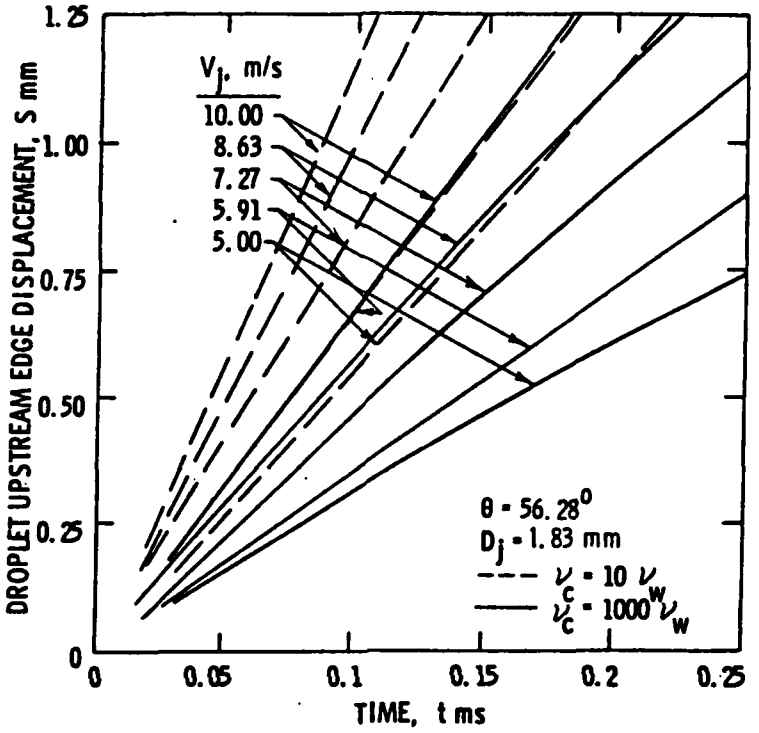

Figure 19. Displacement of Droplet Upstream Edge, S, vs. Time after Commencement of Jet Flow, t, for Various Jet Velocities, V_j

5.1.5 An Effective and Efficient Means to Improve Jet Performance. We have shown in the previous two subsections that an increase of either jet velocity or jet size can improve the cleaning speed. Now we investigate which is more advantageous to improve the cleaning speed for a given jet flow rate ($\dot{Q} = V_j D_j$) by increasing the jet velocity or by increasing the jet size. To evaluate the computed results we first compare curve "a" with curve "a*" in Figure 23 or Figure 24. As listed at the right corners of the figures, both curves correspond to the same flow rate $\dot{Q} = 0.0183\ m^3/s$, however, curve "a" is for a jet velocity twice that of curve "a*" and a jet size half that of curve "a*". A comparison between them reveals that a higher jet velocity produces a higher cleaning speed. This is also true when we compare curve "$\bar{a}$" with "$\bar{a}$*", curve "b" with curve "b*", or curve "$\bar{b}$" with curve "$\bar{b}$*", all for different combinations of V_j and D_j. In the previous two subsections and Figure 20, we also have seen that the efficiency of jet fluid usage can be raised by increasing the jet velocity,

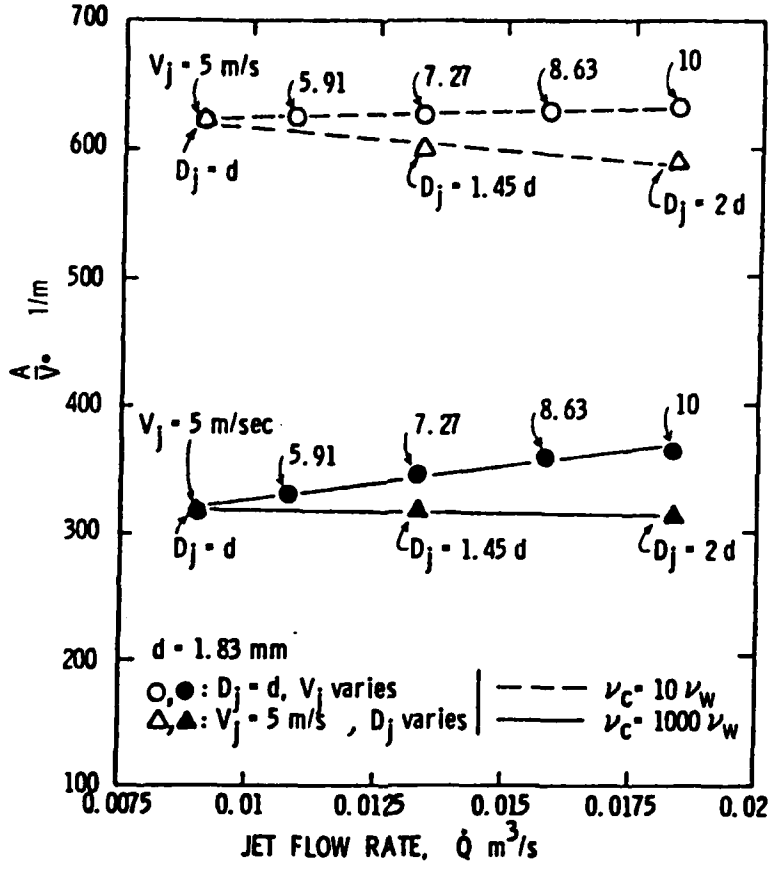

Figure 20. Nominal Area Cleaned Per Unit Volume of Jet Fluid Consumed, A/V^*, for Various Jet Flow Rates, Q

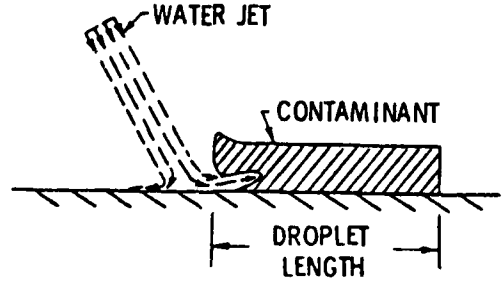

Figure 21. Flow Developing from an Insufficient Jet Size

but not by enlarging the jet size. Therefore, it is more advantageous to increase the jet velocity than the jet size. An important consequence for practical use is that a jet spray composed of a number of small high-speed jets is more effective and more efficient than a single large low-speed jet with the same flow rate.

5.1.6 Pressure Distribution on Impingement Wall. Figure 25 shows some instantaneous pressure distributions on the impingement wall. The peak pressure can be more than 11 times the corresponding steady-state stagnation pressure of the jet, $(1/2)\rho_w V_j^2$. The high pressure may be of concern if the wall can only withstand a limited impact force.

5.2 One-Fluid Flow

In the one-fluid model we set the physical properties (density and viscosity) of the jet fluid equal to that of the contaminant. Then, the interaction between the jet and the contaminant becomes a flow phenomenon that takes place within a single fluid. To justify this treatment, we only examine the viscosity effect because the densities of water and contaminant are approximately equal. For this purpose we computed several flow cases using the two-fluid model and tested the sensitivity of the results to the viscosity of the jet fluid (water).

Figure 26 presents the flow patterns resulting from two viscosity values of jet fluid, $\nu_w = 0.98$ mm^2/s (water) and $\nu_w = 98$ mm^2/s (same as the contaminant viscosity). Figure 27 shows the same cases when the water layer over the droplet is increased from 0.2 mm (used in Figure 6) to 1 mm. The flow patterns in the left and the right hand columns are very similar in all cases. Table 2 summarizes the displacements S and the mean velocities $\dot{S}$ of droplet upstream edge as functions of time for the flow shown in Figure 26. Despite a drastic variation in the viscosity of the jet fluid, the difference in the mean velocities $\dot{S}$ is only of the order of 10 - 15%. A difference of this magnitude is not important because the mean velocity at the early stage (at 0.15 ms) is so large ($\dot{S} > 2.7$ m/s, see Table 2) that practically the droplet is displaced almost instantly after application of the jet. The insensitivity of the flow to the viscosity of jet fluid justifies the use of the one-fluid treatment. Contrary to the jet viscosity, the contaminant viscosity is important as presented in the following. It should be noted, however, that this flow treatment is not suitable if the impact point of the jet is located far away from the droplet. In that case, a thick viscous layer will develop in front of the droplet causing a far shorter displacement of the droplet than by a less viscous jet.

5.2.1 Flow Patterns and Viscosity Effects. Figure 28 presents a sequence of flow developments following the initiation of the jet impingement in Figure 1b. The stream first spreads out on the wall and then

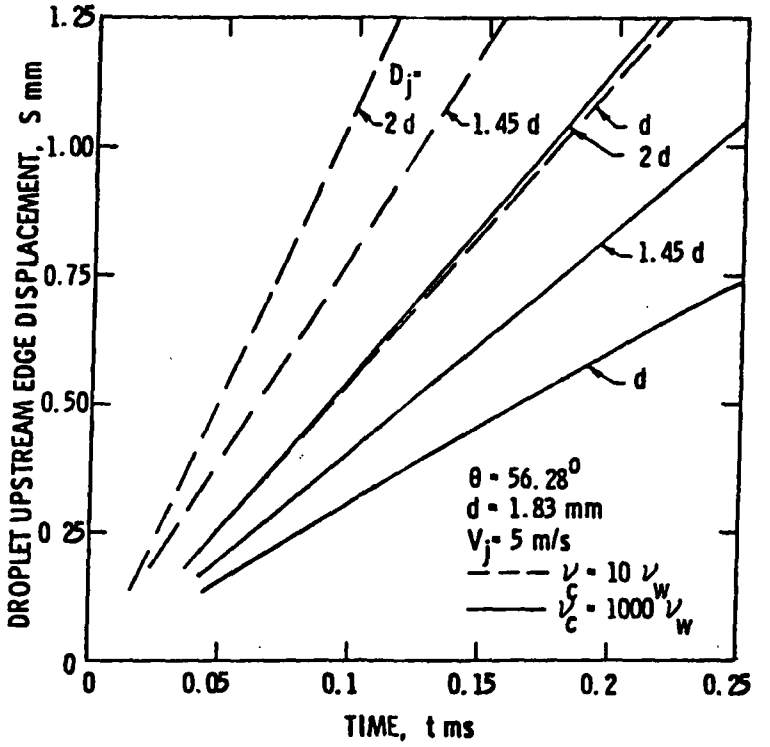

Figure 22. Displacement of Droplet Upstream Edge, S, vs. Time after Commencement of Jet Flow, t, for Various Jet Sizes, D_j

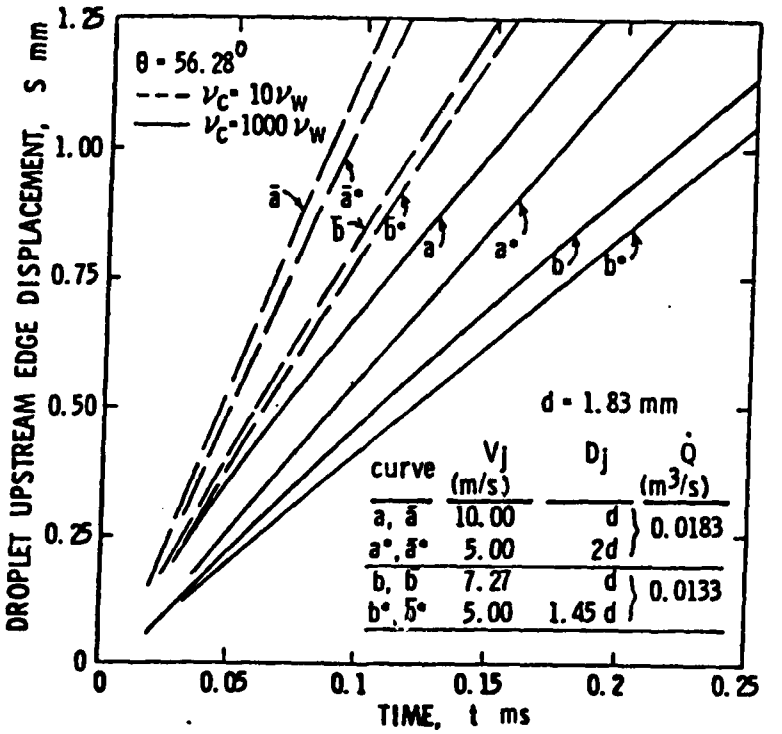

Figure 23. Displacement of Droplet Upstream Edge S, vs. Time after Commencement of Jet Flow, t, for Various Combinations of Jet Velocity, V_j, and Jet Size, D_j

engages the droplet and finally is lifted off the wall. The profile of the jet-contaminant interface cannot be identified in the figure as a result of

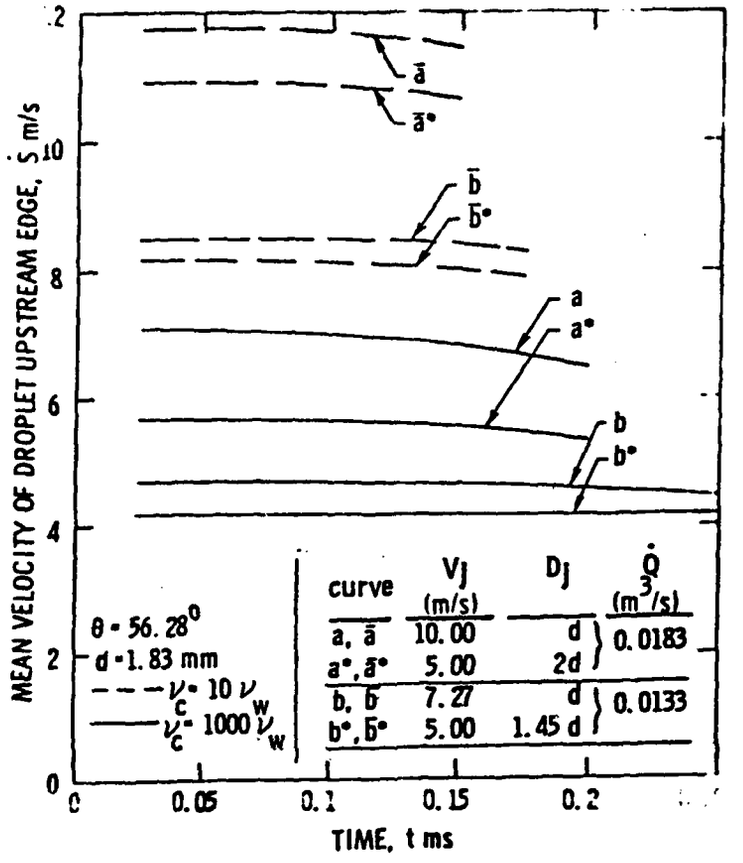

Figure 24. Mean Velocity of Droplet Upstream Edge, $\dot{S}$, vs. Time after Commencement of Jet Flow, t, for Various Combinations of Jet Velocity, V_j, and Jet Size, D_j

the one-fluid treatment. However, by embedding marker particles in the droplet region we are able to track the interface. The map of the marker particles in the case of Figure 28 is presented in the first column of Figure 29. Other columns correspond to increased fluid viscosities. Evidently, the viscosity has a strong effect on the profile and the displacement of the droplet. The viscosity does smoothen out the interface and retards the movement of the contaminant. Another interesting phenomenon we have found is that even if the contaminant viscosity is as small as 9.8 mm^2/s (i.e., 10 times water viscosity), the downstream end of the droplet remains unchanged in shape and location until a half of the droplet in the front has been broken up or distorted.

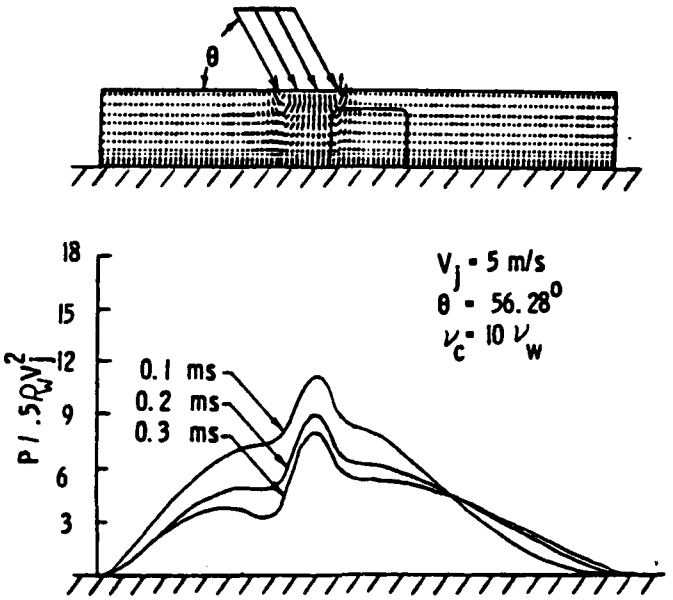

Figure 25. Pressure Distribution on Impingement Wall

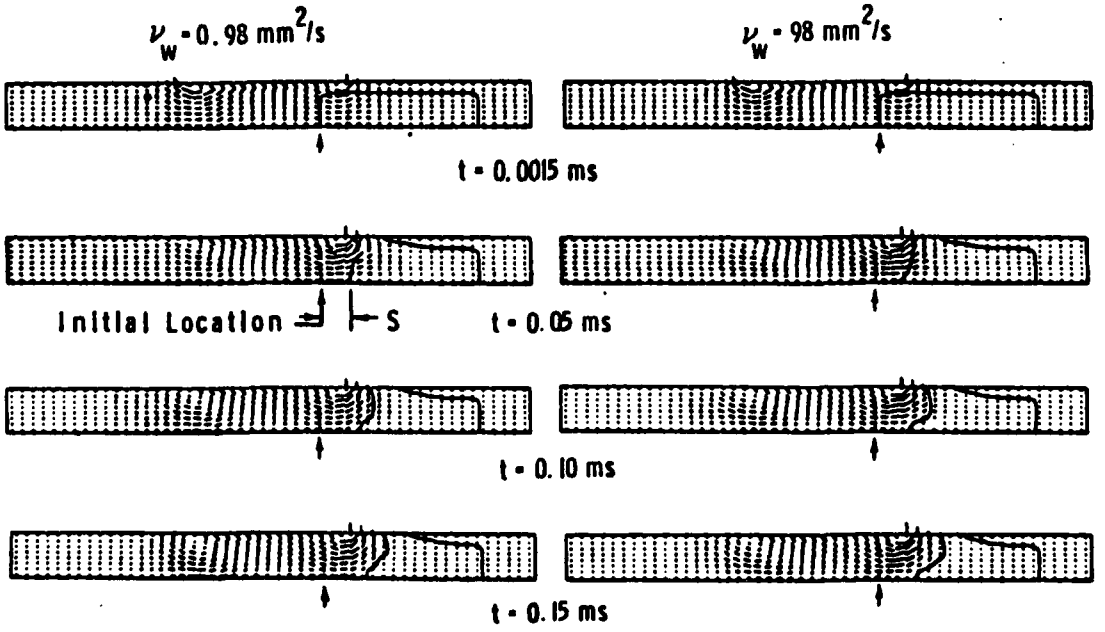

Figure 26. Flow Patterns (Two-Fluid Flow, Thickness of Water Layer above Droplet = 0.2 mm, ν_c = 98 mm^2/s, V_j = 10 m/s, θ = 45°)

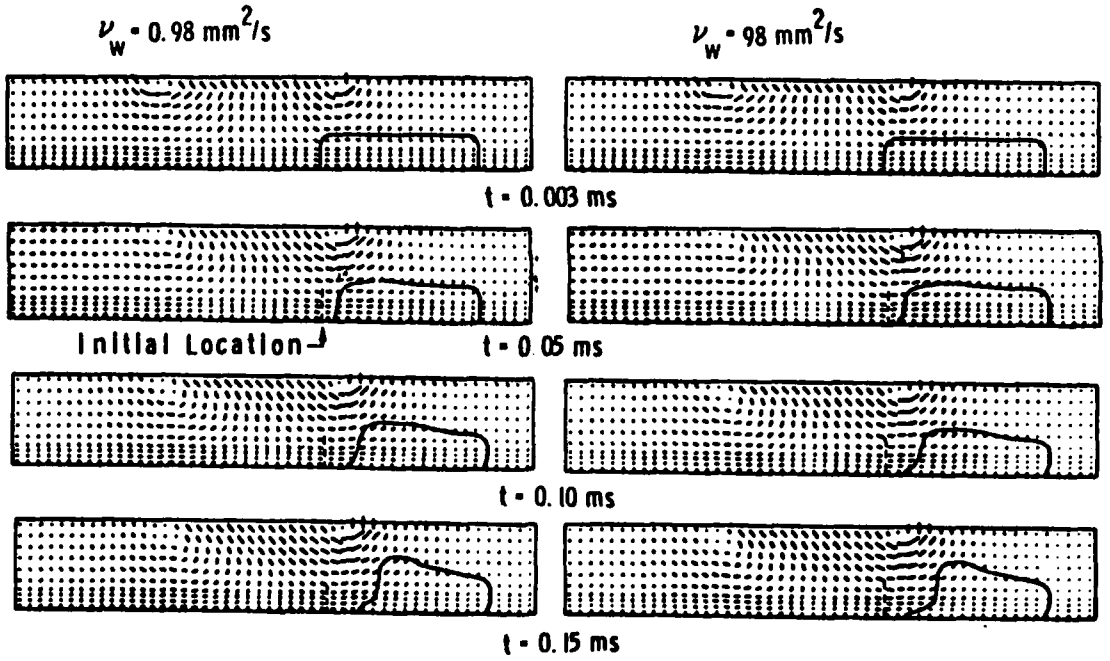

Figure 27. Flow Patterns (Two-Fluid Flow, Thickness of Water Layer above Droplet = 1 mm, ν_c = 98 mm^2/s, θ = 45°)

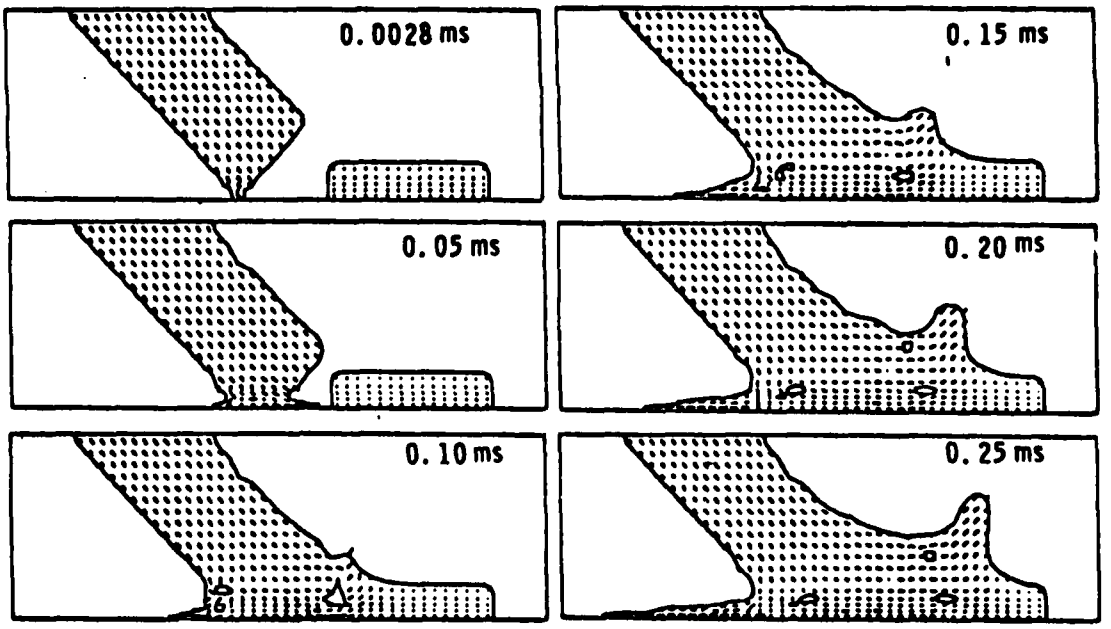

Figure 28. Flow Development (One-Fluid Flow, V_j = 10 m/s, $\nu_w = \nu_c$ = 9.8 mm^2/s, θ = 45°)

Table 2. Displacement S (mm) and Mean Velocity $\dot{S}$ (m/s) of Droplet Upstream Edge vs. Time after Commencement of Jet Flow for Real and Ficticious Viscosities of Jet Fluid ν_w

$\nu_c = 98\ mm^2/s$

V_j m/s	Time ms	$\nu_w = 98\ mm^2/s$		$\nu_w = 0.98\ mm^2/s$		$\frac{\dot{S}_2 - \dot{S}_1}{\dot{S}_2}$ %
		S_1 mm	$\dot{S}_1$ m/sec	S_2 mm	$\dot{S}_2$ m/sec	
5	0.05	0.207	4.13	0.214	4.28	3.4
	0.10	0.422	4.22	0.436	4.36	3.2
	0.15	0.552	3.68	0.597	3.98	7.5
10	0.05	0.467	9.3	0.52	10.04	10.2
	0.10	0.624	6.24	0.727	7.27	14.1
	0.15	0.642	4.28	0.761	5.07	15.6

$\nu_c = 980\ mm^2/s$

V_j m/s	Time ms	$\nu_w = 980\ mm^2/s$		$\nu_w = 0.98\ mm^2/s$		$\frac{\dot{S}_2 - \dot{S}_1}{\dot{S}_2}$ %
		S_1 mm	$\dot{S}_1$ m/sec	S_2 mm	$\dot{S}_2$ m/sec	
5	0.05	0.150	3.04	0.17	3.42	11.1
	0.10	0.280	2.80	0.32	3.20	12.5
	0.15	0.409	2.73	0.445	2.97	8.1
10	0.05	0.257	5.14	0.305	6.10	16.0
	0.10	0.510	5.10	0.580	5.80	12.1
	0.15	0.54	3.60	0.620	4.13	13.0

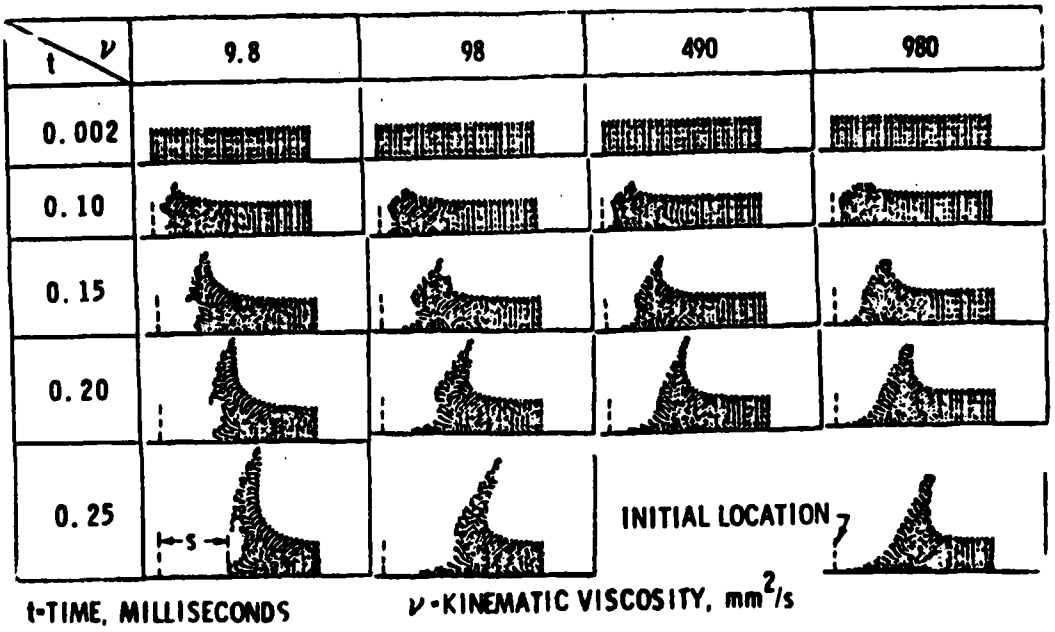

Figure 29. Evolution of Droplets Corresponding to Various Viscosities (One-Fluid Flow, $\theta = 45°$)

5.2.2 **Effects of Jet Velocity and Jet Size on Jet Performance.** Figure 30 presents the displacements S versus time for the fluid viscosity $\nu_c = \nu_w = 98$ mm^2/s and the angle of jet incidence $\theta = 45°$. The jet stream at a higher velocity engages the droplet earlier and thus displaces its upstream edge farther at a given time after the impingement. If the time is measured from the moment at which the displacement starts, then the origins of all three curves in Figure 30 coincide as shown in Figures 31 and 32. In these figures, the three dashed lines are derived from the three solid lines and represent mean velocities $\dot{S}$ of the droplet upstream edge as functions of S and t. They show that an increase of the jet velocity greatly improves the jet performance.

Figures 33 and 34 show flow patterns for $\theta = 0°$ and two jet sizes, $D_j = D$ and $D_j = 2.5\ D$, respectively, where D = 0.6 mm, same as the height of the droplet. We observe that the additional amount of jet fluid from a larger jet size does not provide a significant gain in droplet displacement, but simply flows over the droplet. We have not conducted investigations of cases with $\theta > 0°$, but it can be reasonably expected that at the same jet flow rate, a jet with a higher velocity will outperform a jet with a larger

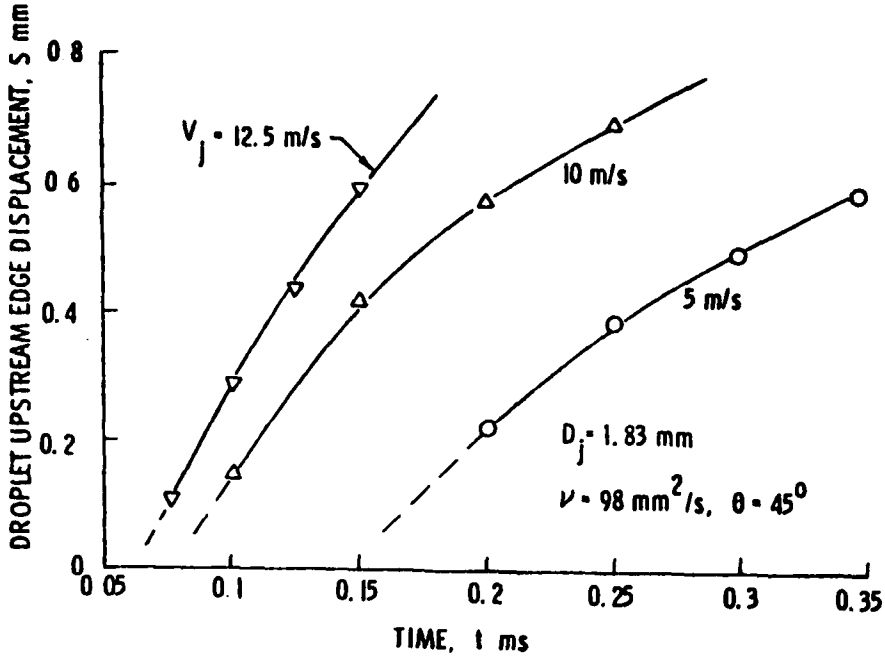

Figure 30. Displacement of Droplet Upstream Edge, S, vs. Time after Commencement of Jet Flow, t (One-Fluid Flow)

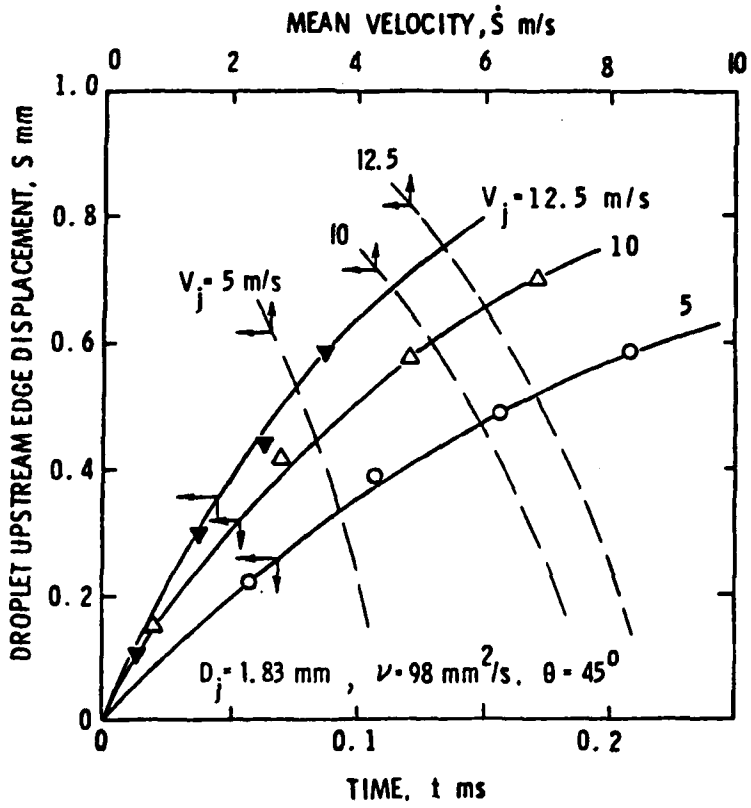

Figure 31. Displacement of Droplet Upstream Edge, S, vs. Time t, and Mean Velocity Ṡ, vs. S

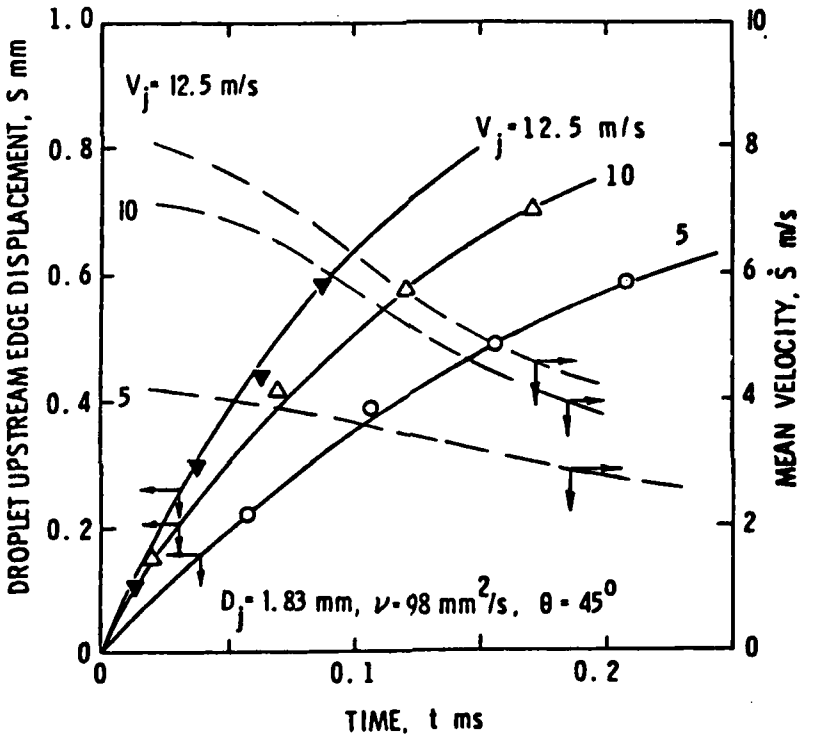

Figure 32. Displacement S and Mean Velocity $\dot{S}$ of Droplet Upstream Edge vs. Time after Displacement S takes place

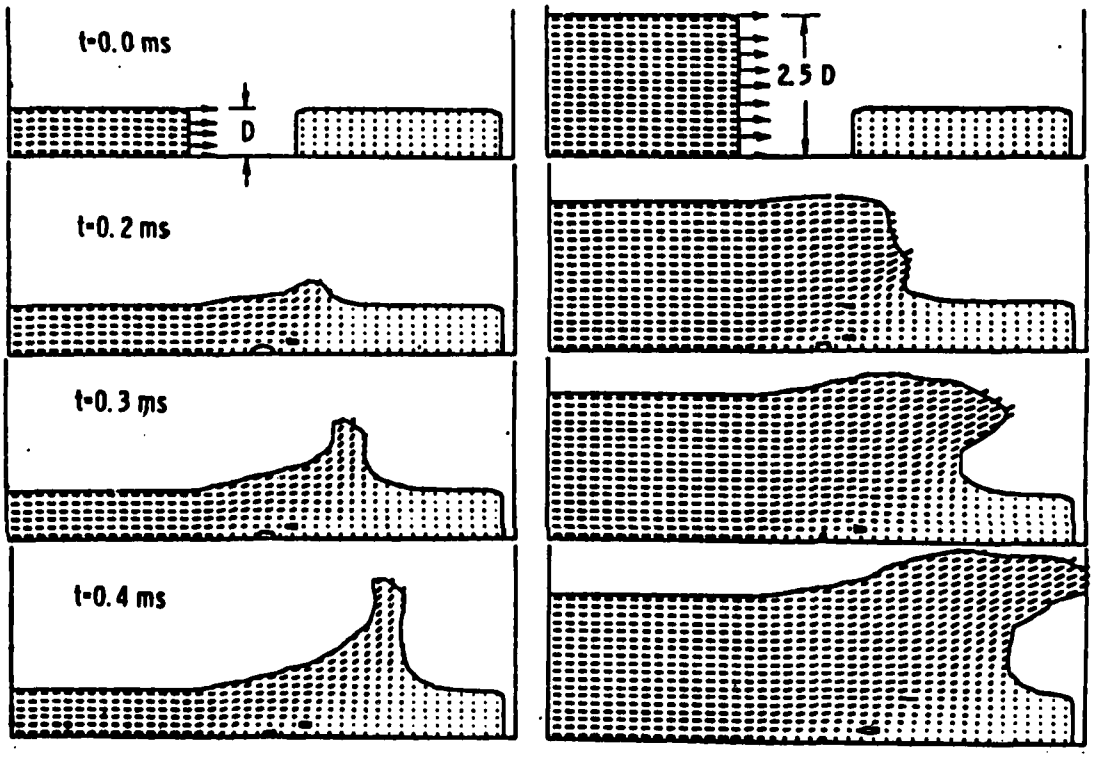

Figure 33. Comparison of flow Developments between Two Jet Sizes, Dj = D and 2.5D (One-Fluid Flow, $\nu_w = \nu_c$ = 9.8 mm/s, V_j = 10 m/s, $\theta = 0^o$, D = 0.6 mm)

size. This is the same conclusion as in the case that the droplet was initially covered with water.

5.2.3 **Pressure Distribution on Impingement Wall.** The computed pressure distributions on the wall for various times are shown in Figure 35. Their maximum value is twice the steady-state stagnation pressure of the jet. This is much lower than the pressure shown in Figure 25 in which the droplet was initially covered by a water layer.

VI. JET-CONTAMINANT INTERACTIONS IN CONFINED GEOMETRIES

In the following we will briefly examine flow interactions taking place in confined geometries other than the plane wall. The geometries considered are cavities in a wall and corners of two perpendicular walls shown in Figures 36 and 37. The basic difference between the cavity and the corner is that in a cavity there is no flow through the left boundary of the flow region. In each geometry, two values, $\theta = 45°$ and θ 90°, were used for the angle of jet incidence. The contaminant in the confined geometries initially can be in form of a droplet or covers the entire bottom surface with a thin water layer above it. The two-fluid model was used for flow calculation. We now present the computer-generated flow patterns and typical pressure distributions on the bottom surfaces of the geometries.

6.1 Flow Patterns.

6.1.1 **Interactions in Cavities.** Figure 38a shows the flow generated by a water jet impinging on the upper surface of the cavity filled with water and a contaminant droplet located at the corner, as depicted in Figure 37a. All of the following computer-generated plots have been magnified three times in the vertical direction. The plots in the left and the right columns correspond to the 45° and 90° impingement, respectively. The figure shows that the angle of incidence has a profound effect on the flow direction and accordingly, the movement of the droplet. In the 45°-impingement, the main stream tends to move toward the wall on the other side of the cavity before it exits the region, while in the 90°-impingement, a large fraction of the jet stream exits the cavity right next to the entrance region of the jet stream. At 0.3 ms there is a small amount of contaminant stagnating at the right corner in the 90° case, but not in the 45° case. The jet impinging at 45° seems to have more cleaning power for decontamination of the cavity. There are two vortexes seen in the flow field, one adjacent to the entrance of the jet and the other inside the droplet. The second vortex can be clearly identified in Figure 38b.

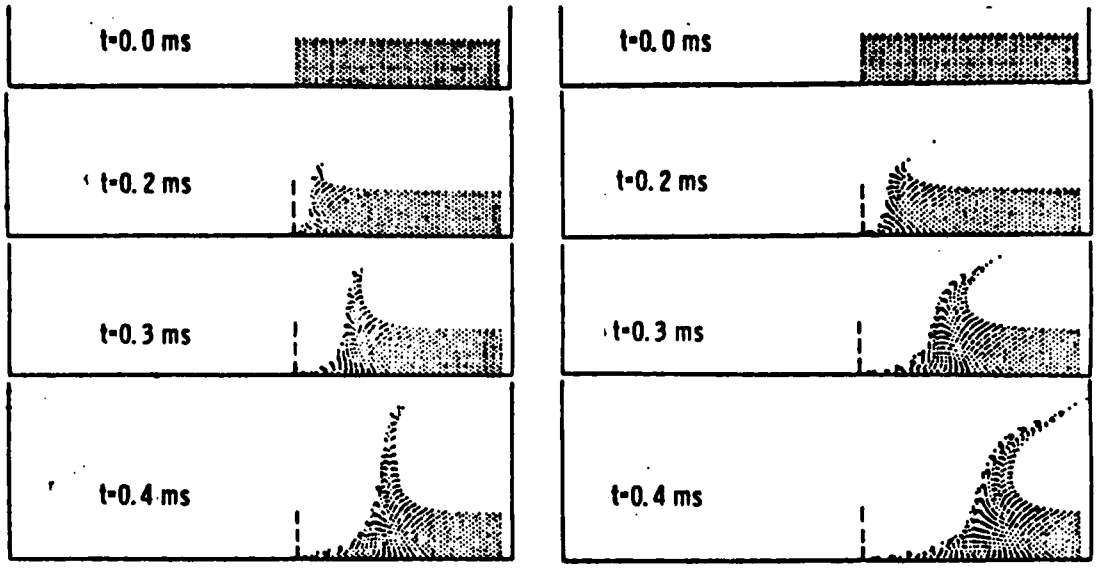

Figure 34. Evolution of Droplets Corresponding to Figure 32.

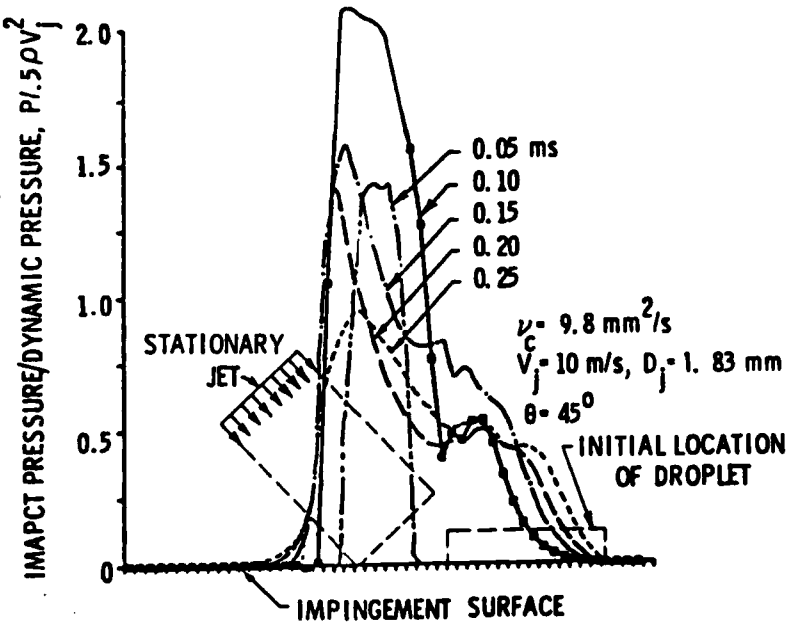

Figure 35. Pressure Distributions on Impingement Wall

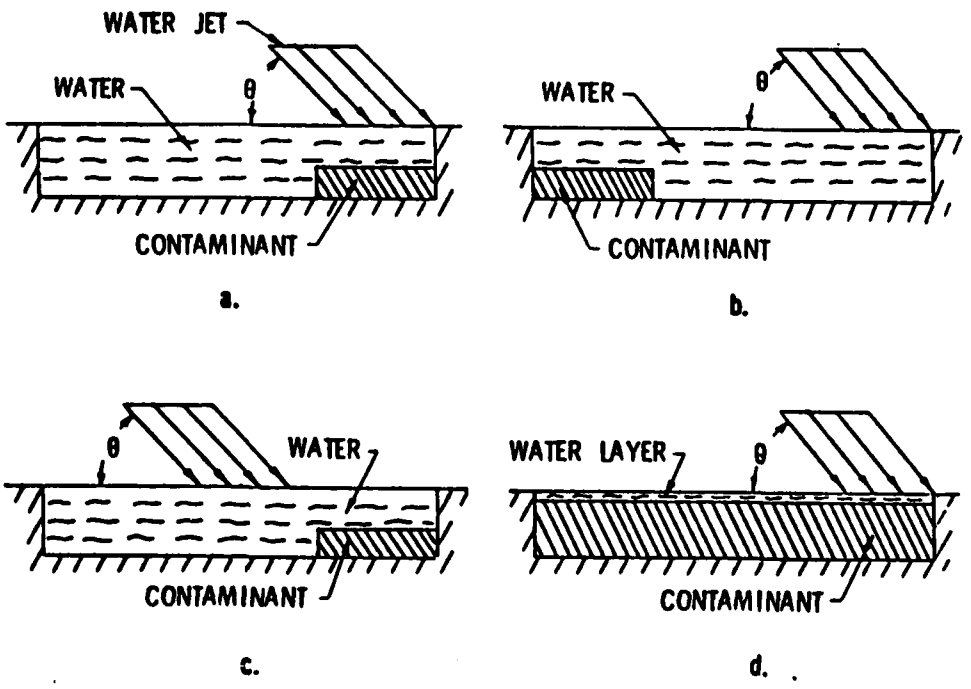

Figure 36. Pre-impingement Flow Configurations in Cavities

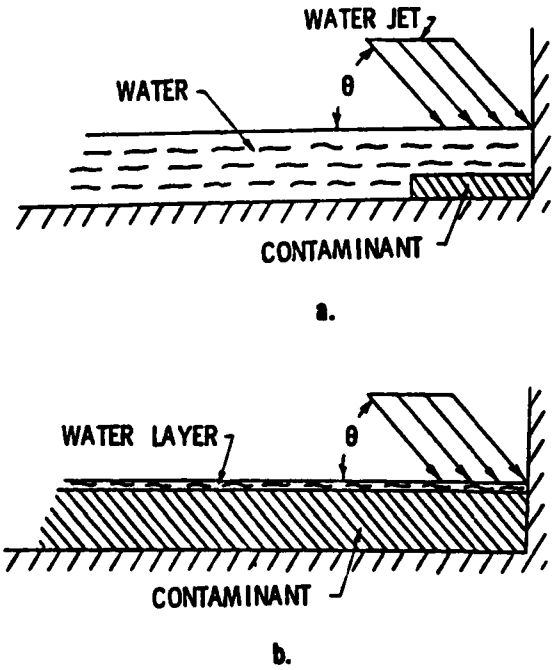

Figure 37. Pre-impingement Flow Configurations at Corners of Two Perpendicular Walls

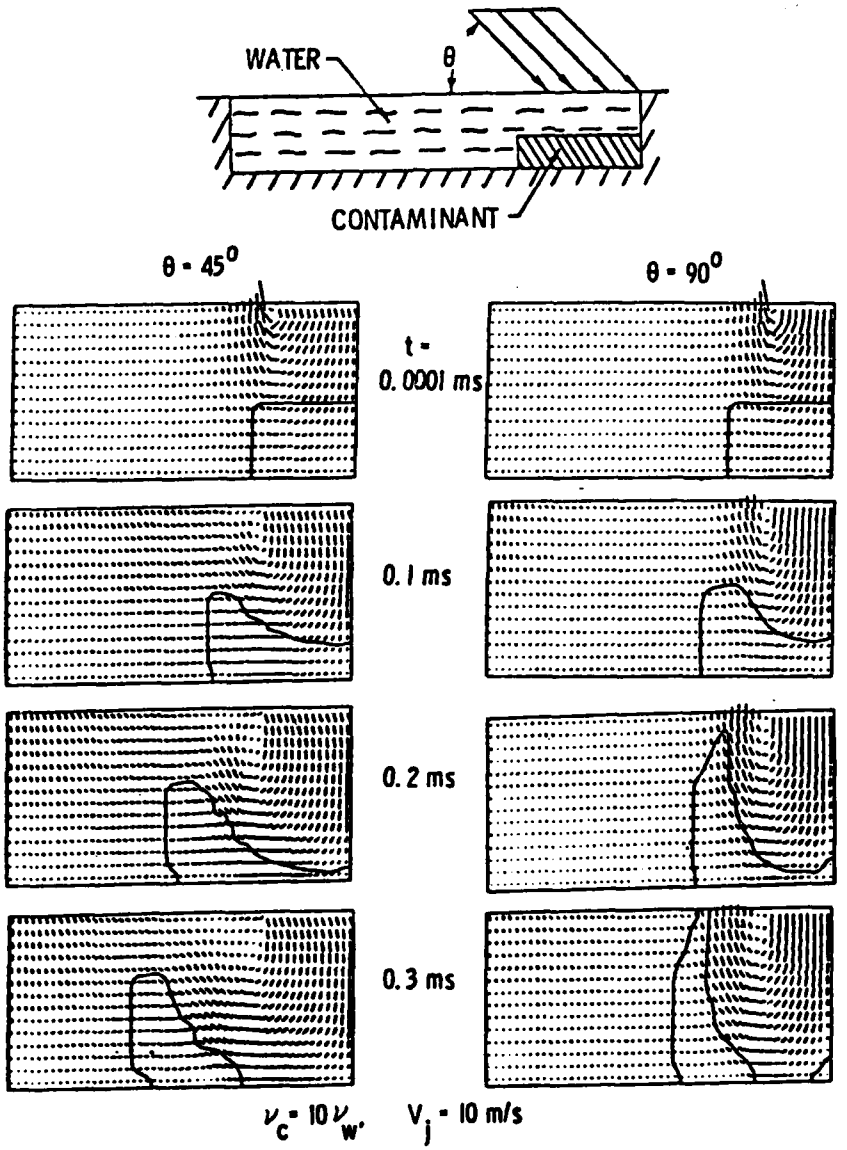

Figure 38a. Flow Developments Corresponding to Figure 36a.

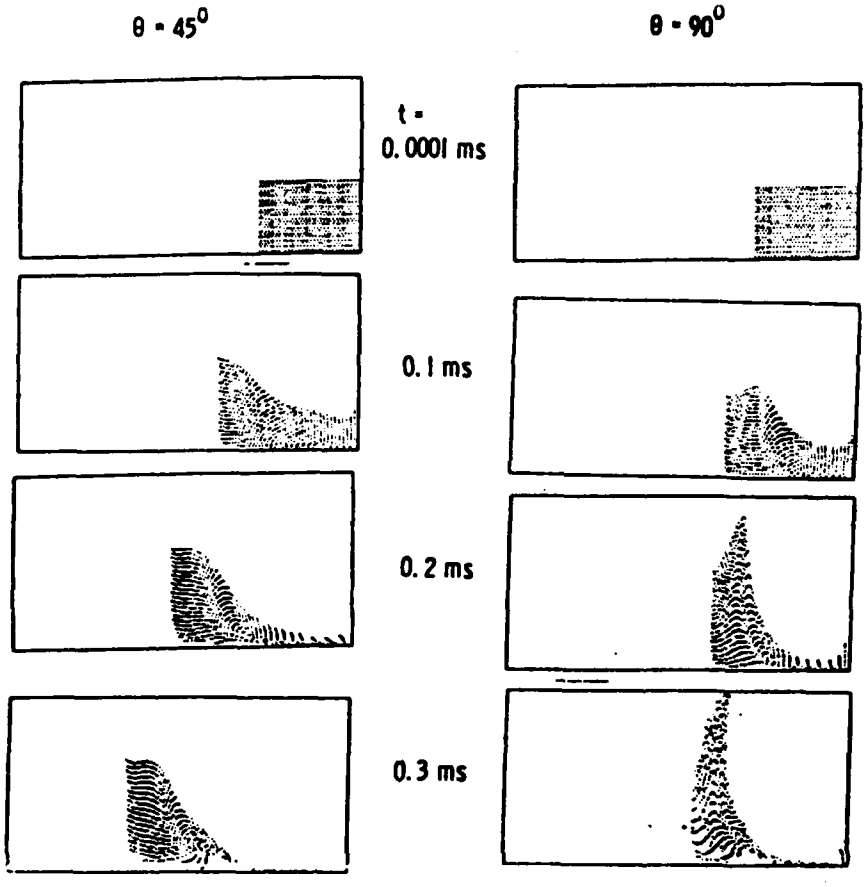

Figure 38b. Evolution of Droplets Corresponding to Figure 38a

If a droplet is initially located at the left end corner of the cavity as depicted in Figure 36b, then again the jet impinging at 45° provides a higher rate of cleaning, as shown in Figures 39a and 39b.

Figures 40a and 40b show another case that the impingement takes place in the central part of the cavity. In the 90°-impingement, the main stream of the jet does not extend far enough to the vertical walls, causing only little movement of the contaminant along the wall.

Figure 41 shows flow developments corresponding to the configuration in Figure 36d in which the cavity is initially filled with contaminant covered by a thin water layer. The jet impinging at 90° appears to have more power to displace the contaminant at very early times. However, this superiority disappears after $t > 0.18$ ms as a result of a faster development of viscous layer along the vertical wall for $\nu = 90°$.

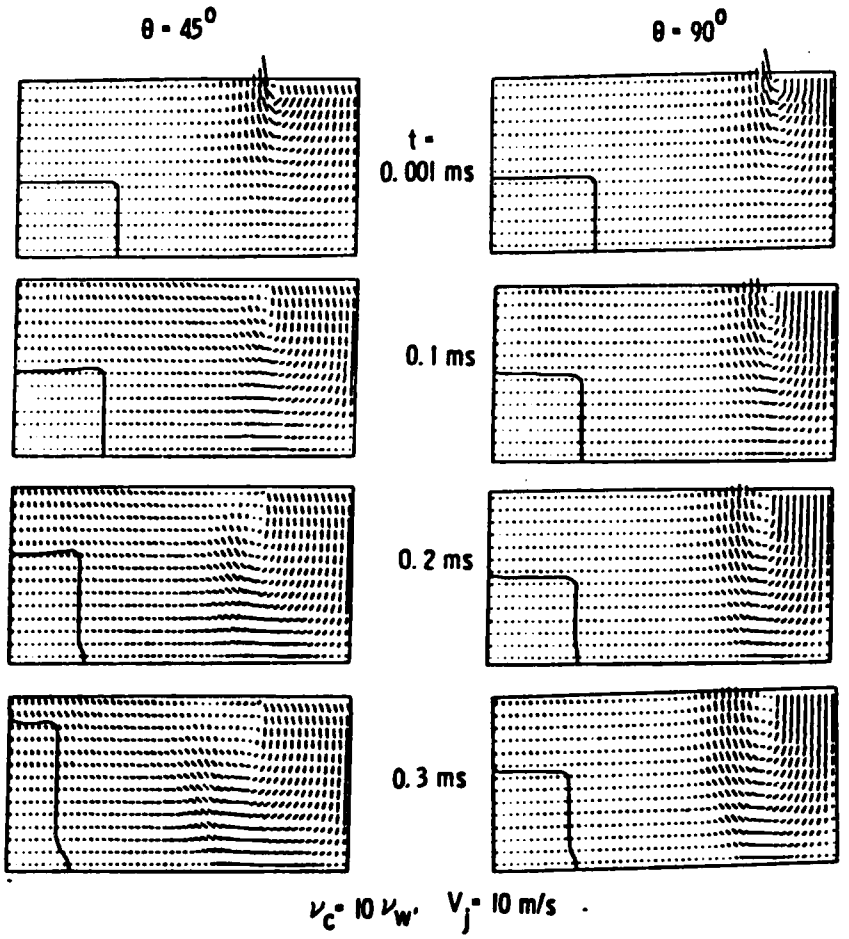

Figure 39a. Flow Developments Corresponding to Figure 36b

6.1.2 Interactions at Corners of Two Perpendicular Walls

Figures 42 and 43 show flow developments corresponding to the configurations of Figures 37a and 37b, respectively. Both 45° and 90° result in similar flow patterns except that there is a small amount of contaminant stagnating at the corner in the 90°-impingement.

In summary, we conclude from the flow patterns presented that an inclined jet impingement is more effective for decontamination in various confined geometries.

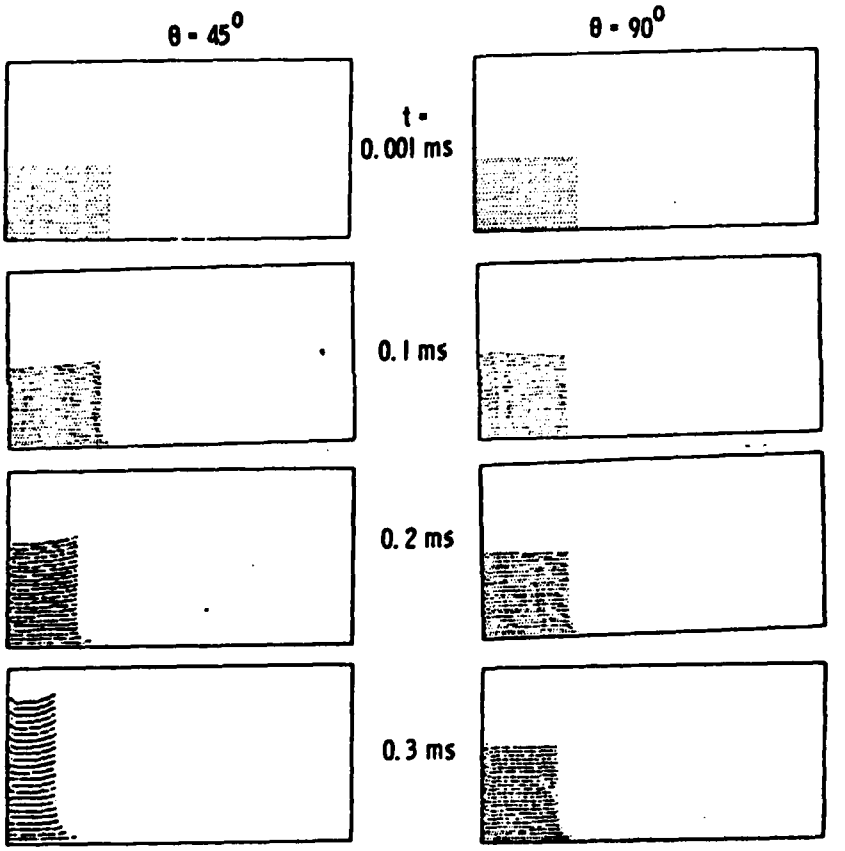

Figure 39b. Evolution of Droplet Corresponding to Figure 39a

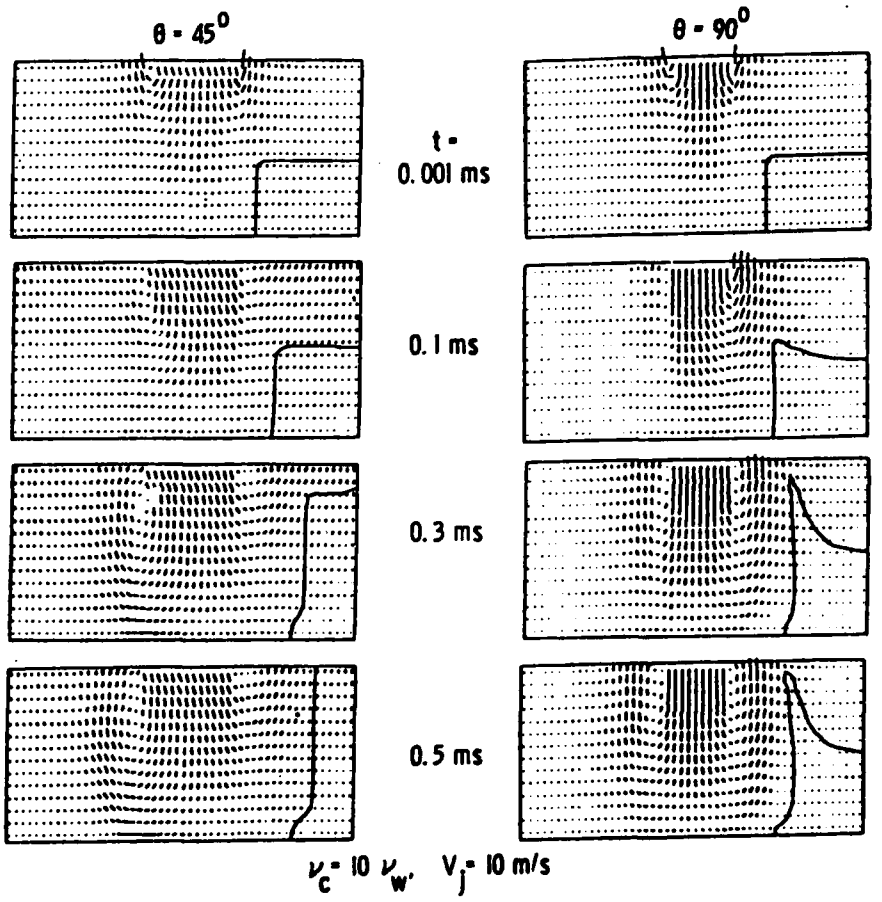

Figure 40a. Flow Developments Corresponding to Figure 36c

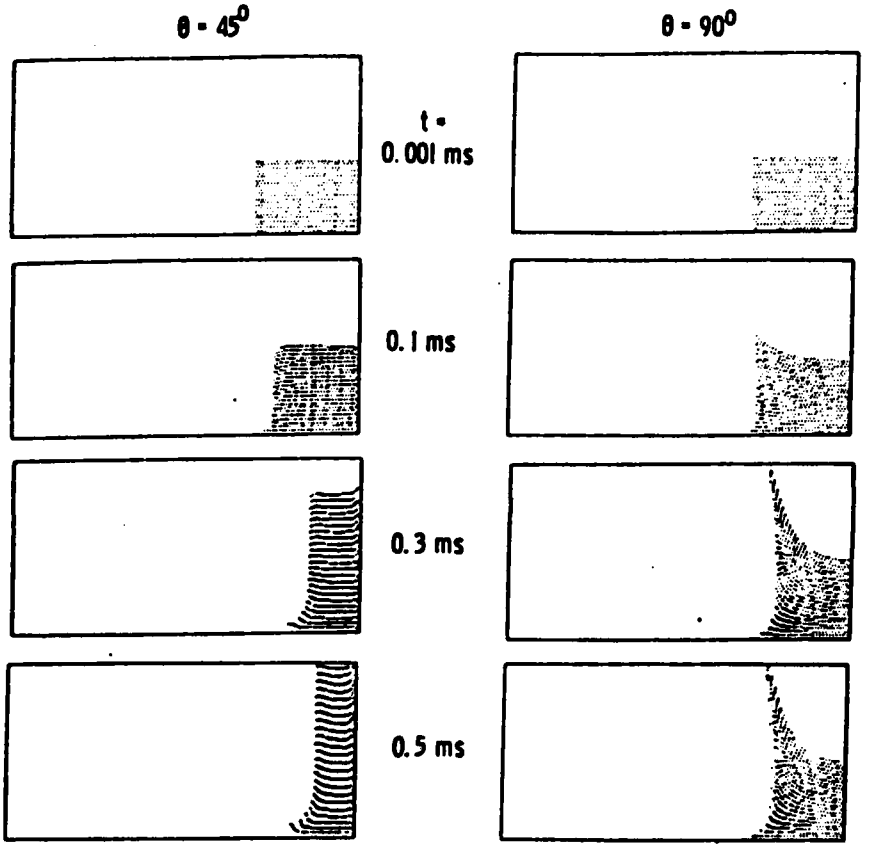

Figure 40b. Evolution of Droplets Corresponding to Figure 40a

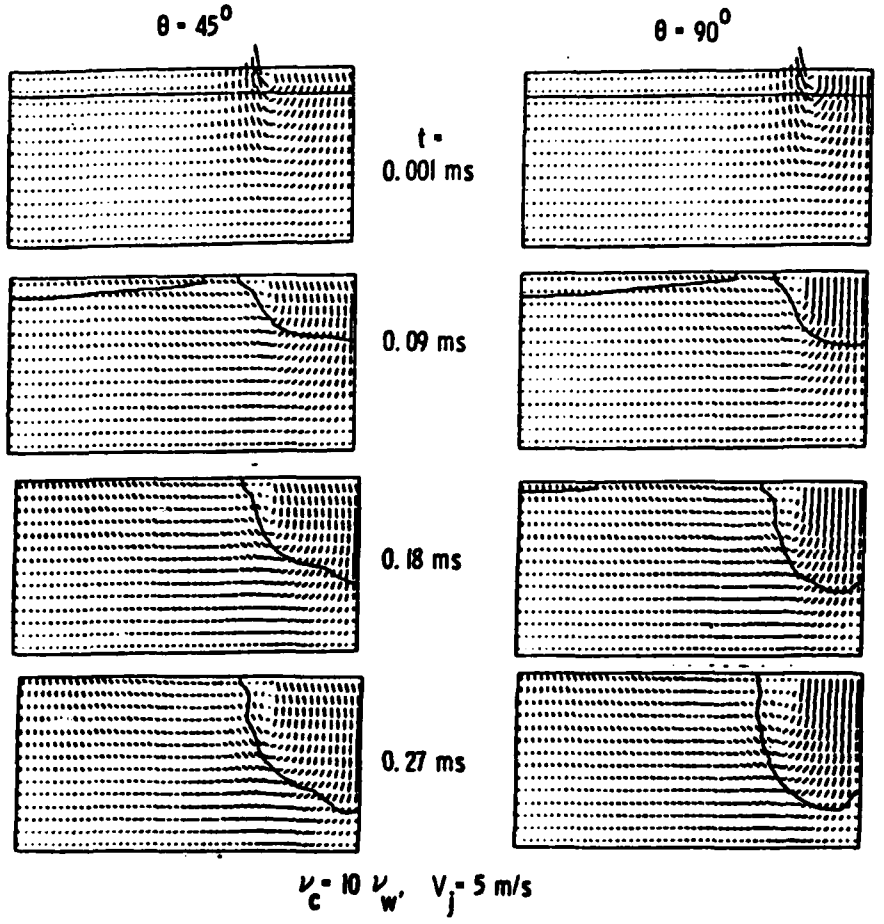

Figure 41. Flow Developments Corrseponding to Figure 36d

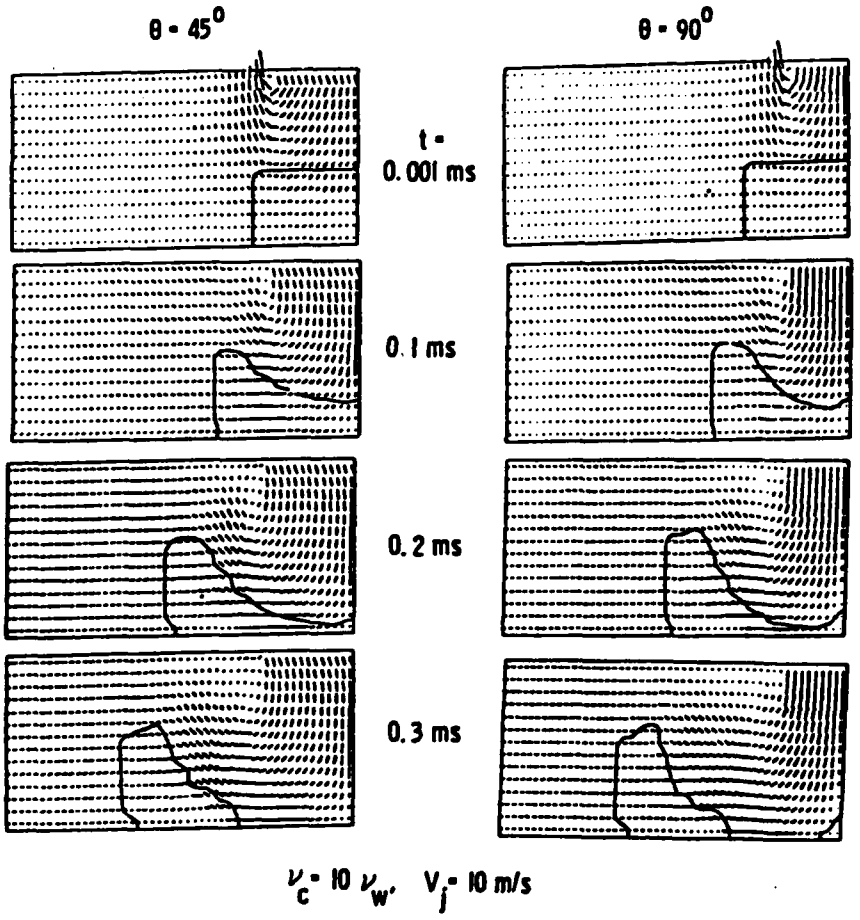

Figure 42a. Flow Developments Corresponding to Figure 37a

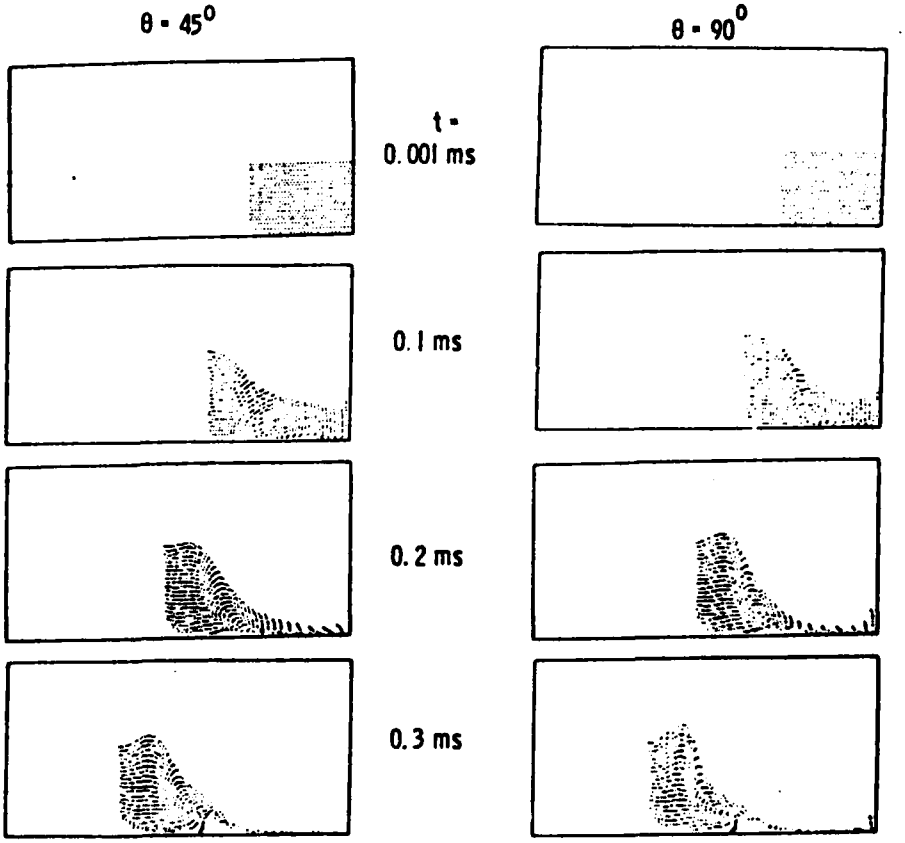

Figure 42b. Evolution of Droplets Corresponding to Figure 42a

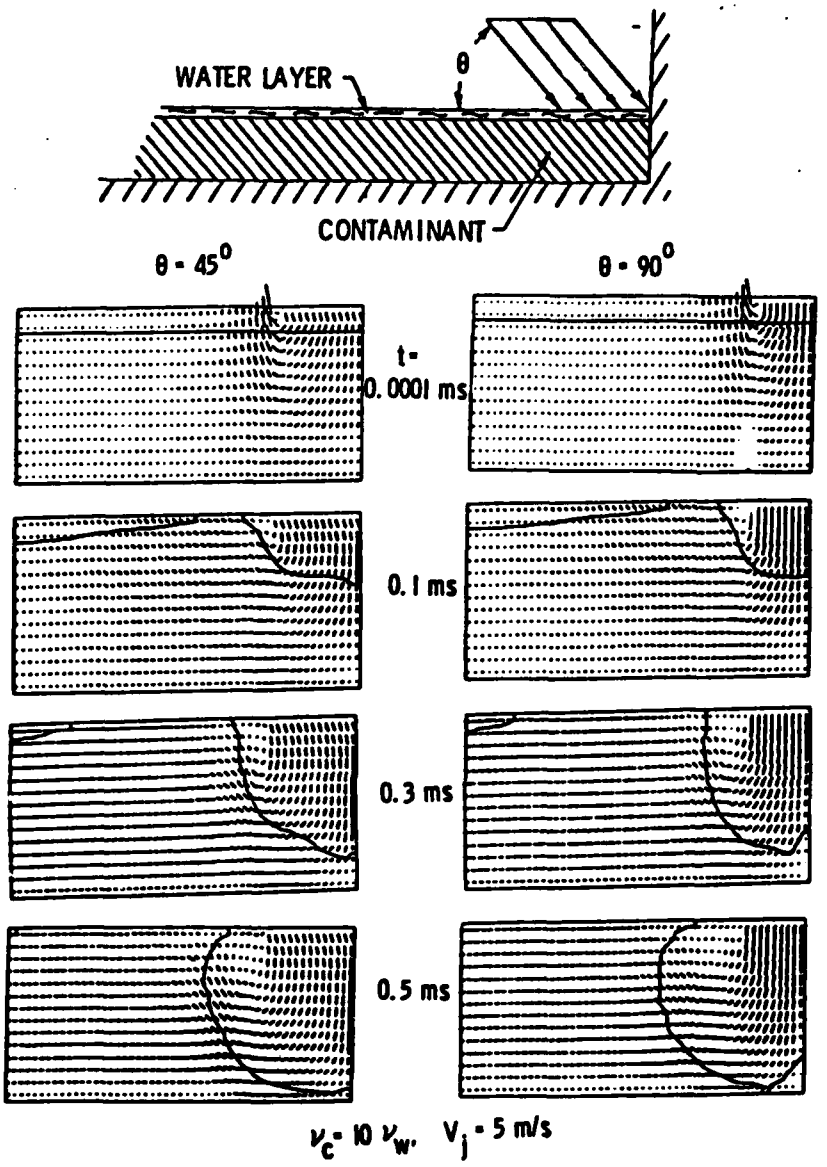

Figure 43. Flow Developments Corresponding to Figure 37b

6.2 Pressure Distribution on Bottom Surfaces of Confined Geometries

Figures 44 through 47 present the instantaneous pressure distributions on the bottom walls in the flow cases discussed above. In any flow case, the peak pressure far exceeds the corresponding steady-state stagnation pressure of the jet. With the same contaminant configuration, the pressure rise is relatively higher in cavities than at corners as a result of more flow confinements in cavities. In general, the pressure rise in a confined geometry is a function of the dimension ratio of the jet to the geometry, the amount of contaminant originally resided, the contaminant viscosity, the location of jet impingement, the angle of jet incidence, and so forth.

VII. GENERAL REMARKS

The following general remarks can be made based on the results reported in the previous chapters.

7.1 Application of Air Jets

A great advantage of decontamination by air jets is that there is no shortage in the supply of jet fluid (air). However, air jets are less effective in comparison with water jets because of the much lower air density which produces a much smaller impingement force on the contaminant. Because air density is only 0.0012 of water density in atmosphical pressure, the air speed has to be 286 m/s in order to produce a dynamic pressure equivalent to that of water jets at 10 m/s. The jet at such a high speed may constitute a noise hazard. In addition, often there are contaminant stains left on the surface cleaned by air jets.

7.2 Arrays of Jets

In Chapter V we concluded that at a given jet flow rate a small high-speed jet provides a larger cleaning speed and consumes less jet fluid than a large low-speed jet. To clean a large area, it is reasonable to assemble a number of small high-speed jets in arrays to preserve their superior performance.

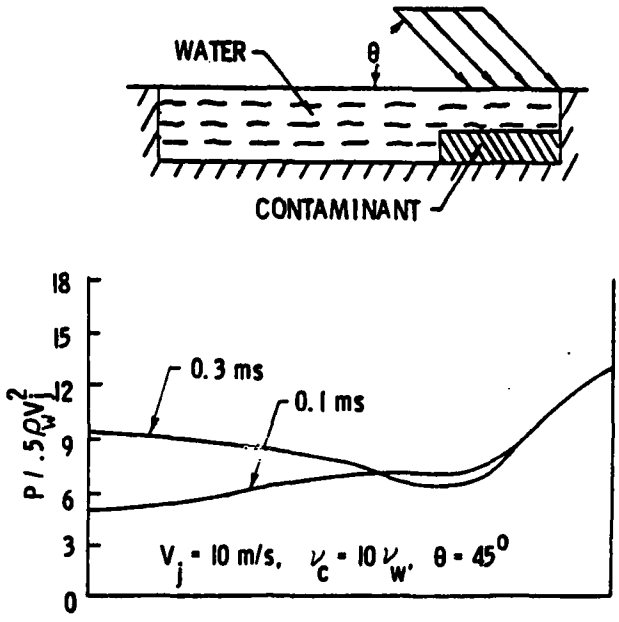

Figure 44. Pressure Distributions on Bottom Wall Resulting from Impingement of Figure 36a

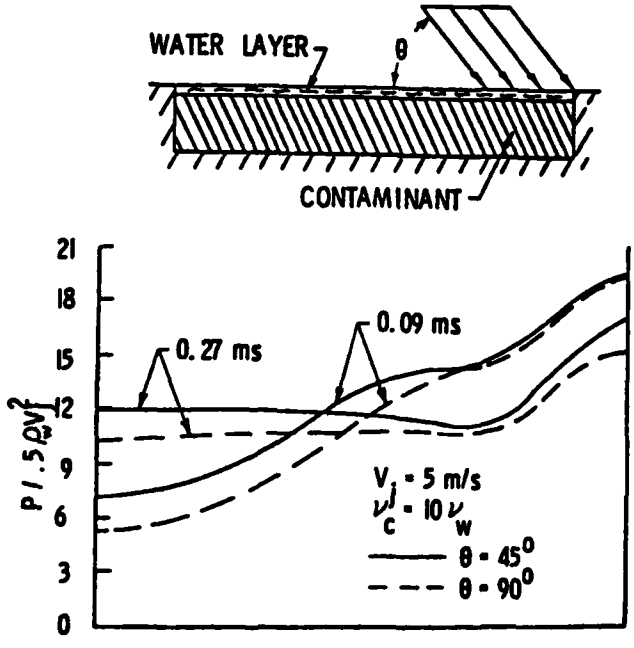

Figure 45. Pressure Distributions on Bottom Wall Resulting from Impingement of Figure 36d

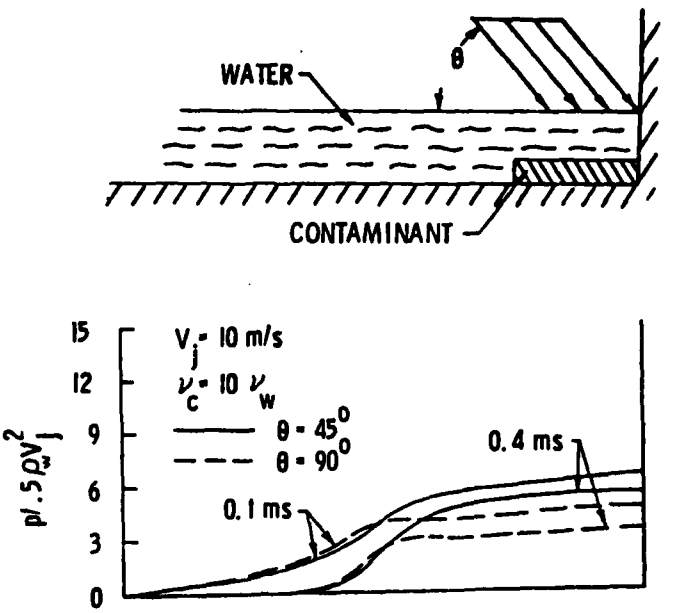

Figure 46. Pressure Distributions on Bottom Wall Resulting from Impingement of Figure 37a

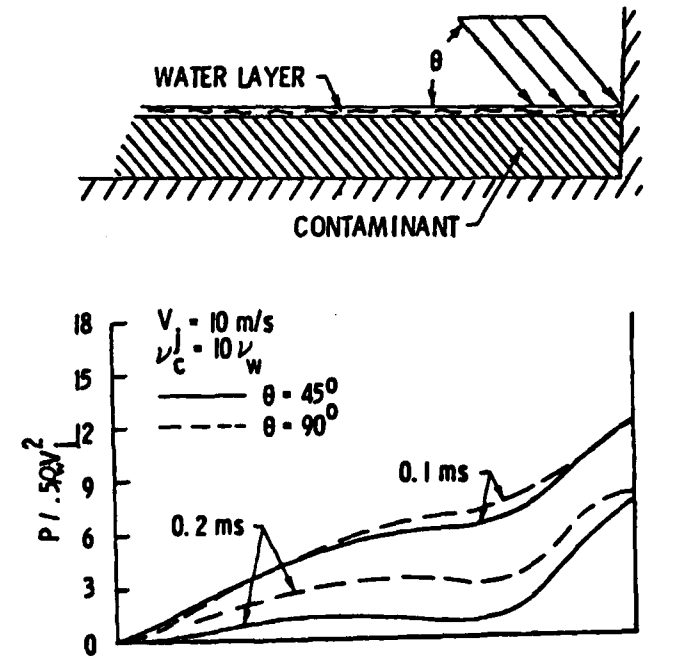

Figure 47. Pressure Distributions on Bottom Wall Resulting from Impingement of Figure 37b

There are many possible arrays of single jets. Depicted in Figure 48 are some general arrangements. Single jets at an inclined angle may be assembled in form of straight lines "a," concaves "a," a circle "c," or convexes "d." The arrangement "a" is effective when the array is moved forward, but not sideways. The arrangement "b" will push the contaminant to the central region and has to carry it all the way when the spray is moved forward. It may perform better than "a" when moved laterally. The arrangement "c" can provide effective cleaning in all directions. The arrangment "d" may have a performance superior to "c" because the impact locations of the jets in the two rows in "d" can be arranged in an alternate pattern and hence each jet in the array can be used more efficiently. Experiments are needed to test this advantage.

7.3 Justification of Validity of Two-Dimensional Flow Model

The flow from a single round jet impinging on a surface is three-dimensional. If the angle of jet incidence is 90^{o} and the surface is flat and smooth, the fluid uniformly spreads out in all directions. When the jet is inclined gradually, the stream in the lateral direction shrinks and the stream in the front grows accordingly. Eventually, the flow pattern resembles that formed by a two-dimensional jet. Also, when a number of round jets separated by a small distance from each other are arranged in a straight line or in an arc pattern, the resultant flow on a flat surface resembles a two-dimensional flow.

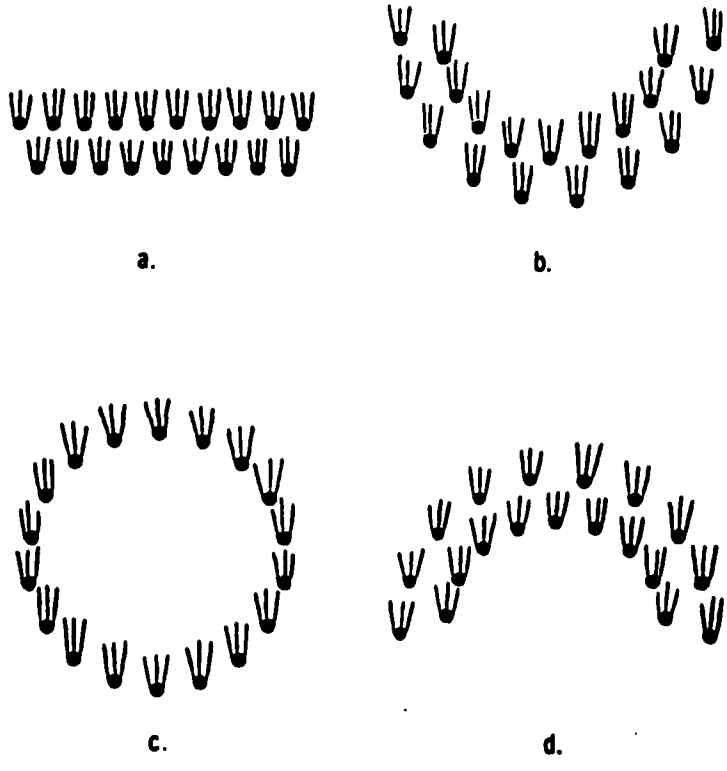

Figure 48. Arrays of Jets

In applications, the jet spray will be composed of a number of single jets assembled as shown in Figure 49 and the jet flow will be directed at an impingement angle less than 90°. Thus, the two-dimensional models developed in Chapter II are suitable for an investigation of fundamental flow characteristics of the interaction between such arrays and contaminant droplets.

7.4 Pulsating Jets

A jet with pulsating flow creates a great transient. Each pulse of the flow acts as an initiation of a new jet flow and the pulsation produces a series of impact pressures on the surface. These impact pressures are much greater than the pressures produced by a continueous jet flow without pulsation, as has been shown in Chapter V. A large impact pressure is particularly helpful to break up and displace hard-to-remove contaminant droplets. The flow interaction involved, however, is extremely complex and it is not clear how the interaction is related to the frequency of pulsation and to other flow parameters. During the period between two adjacent pressure pulses, there is a little or no force acting on the contaminant droplet. It is possible that the contaminant ceases to move or even moves backward if the water layer which covers it is thick and if the frequency of pulsation is not appropriate.

We have attempted to characterize this flow using the SOLA-VOF code, but were unable to obtain reasonable results. The difficulties encountered were the numerical instability and divergence. A modification of the numerical method employed in the code possibly may resolve the problem.

7.5 Simulation of a Moving Jet

In this report we have assumed that the jet is stationary in the physical space. Simulations were also attempted for a jet moving toward the contaminant droplet, but they were not sucessful because of numerical problems. New code development is necessary in order to adapt the SOLA-VOF code to this problem.

VIII. SUMMARY AND CONCLUSIONS

Two flow models, called one-fluid flow and two-fluid flow, have been used to investigate jet-contaminant interactions on a plane wall. Both models represent two-dimensional viscous flows, governed by the Navier-Stokes equations. The computations were done with the SOLA-VOF finite difference code in which we implemented a viscosity relation to adapt the code to handle the present case that the two fluids involved have different viscosities.

The report presents computer-generated flow patterns which show typical flow developments following the jet impingement. It is found that the contaminant viscosity has strong effects on the displacement and the profile of the droplet. In the high viscosity case, a thick viscous layer develops quickly inside the contaminant region and the jet stream is lifted off the wall. As a result, the contaminant with high viscosity is much more difficult to remove. Computed results show that the angle of jet incidence, the jet velocity, and the cross-sectional area of the jet are important parameters that govern the performance of the jet. The results also show that the jet can perform in the most effective and most efficient way in decontamination at an angle of incidence in the range of 45°-60°. Also, it is more advantageous to use a jet spray composed of a number of small high-speed jets than one consisting of a single large low-speed jet.

Jet contaminant interactions taking place in confined geometries, such as cavities and corners of two perpendicular walls, were also examined. The results show that an inclined jet is more effective than a normal jet in confined geometries.

In all flow cases studied, the instantaneous impact pressure on the wall can far exceed the corresponding steady-state stagnation pressure of the jet

ACKNOWLEDGMENTS

This work was supported by the U.S. Army Chemical Research and Development Center (CRDC). The author gratefully acknowledges the assistance of Dr. Joseph E. Matta of CRDC in providing all the information needed for this study.

REFERENCES

1. G. I. Taylor, "Oblique Impact of a Jet on a Plane Surface," Phil. Trans. R. Soc. A, 260, 1966, pp. 96-100.

2. J. H. Mitchell, Phil. Trans. A, 181, 1890, pp. 389-431.

3. A. Rubell, "Computations of Jet Impingement on a Flat Surface," AIAA J,. 18, No. 2, Feb 1980, pp. 168-175.

4. A. Rubell, "Computations of the Oblique Impingement of Round Jets upon a Plane Wall," AIAA J., 19, No. 7, July 1981, pp. 863-871.

5. J. N. Hunt, "Wave Formation in Explosive Welding," Philosophical Magazine, 8th Series, Vol. 17, p. 669-680, 1967.

6. J. M. Vanden-Broeck, "Deformation of a Liquid Surface by an Impingement Gas Jet," SIAM J. Appl. Math., 41, No. 2, Oct 1981, pp. 306-309.

7. B. D. Nicholas, C. W. Hurt, and R. S. Hotchkiss, "SOLA-VOF: A Solution Algorithm for Transient Fluid Flow with Multiple Free Boundaries," Los Alamos Scientific Laboratory Report No. LA-8355, 1980.

8. J. Matta, U. S. Army Chemical Research and Development Center (CRDC), private communication, Jan 1983.

NOMENCLATURE

A	area which has been decontaminated
c	sound speed, Eq. (1)
D	a constant, D=0.6 mm
D_j	thickness of jet (jet diameter in three-dimensional cases)
F	"fractional volume of fluid" function, Eq. (4)
P	pressure
p	pressure, Eq. (1)
q	variable, Eq. (8)
$\dot{Q}$	jet flow rate, m^3/s
S	displacement of droplet upstream edge, mm
$\dot{S}$	mean velocity of droplet upstream edge, m/s
S'	*a constant*, Figure 5
t	time
U	fluid velocity on the wall
u	fluid velocity component, Eq. (1)
u_1	fluid velocity, Eq. (7)
v	fluid velocity component, Eq. (1)
V^*	volume of jet fluid consumed
V_j	jet velocity
x	coordinate, Eq. (1)
x_1	distance, Eq. (7)
y	coordinate, Eq. (1)
θ	angle of jet incidence

NOMENCLATURE

ν kinematic viscosity of fluid mixture, Eq. (1)

ν_c kinematic viscosity of fluid mixture, Eq. (1)

ν_w kinematic viscosity of water

ρ density of fluid mixture, Eq. (1)

ρ_c density of contaminant

ρ_w density of water

Subscripts

c contaminant

j jet

w water

DISTRIBUTION LIST

No. Of Copies	Organization
12	Administrator Defense Technical Info Center ATTN: DTIC-DDA Cameron Station Alexandria, VA 22314
1	Office of the Under Secretary of Defense Research & Engineering ATTN: R. Thorkildsen Washington, DC 20301
1	HQDA/SAUS-OR, D. Hardison Washington, DC 20301
1	HQDA/DAMA-ZA Washington, DC 20310
1	HQDA, DAMA-CSM, E. Lippi Washington, DC 20310
1	HQDA/SARDA Washington, DC 20310
1	Commandant US Army War College ATTN: Library-FF229 Carlisle Barracks, PA 17013
1	Commander US Army Materiel Development and Readiness Command ATTN: DRCDRA-ST 5001 Eisenhower Avenue Alexandria, VA 22333
1	Commander US Army Materiel Development and Readiness Command ATTN: DRCSF-E, Safety Office 5001 Eisenhower Avenue Alexandria, VA 22333
1	Commander US Army Materiel Development and Readiness Command ATTN: DRCDE-DW 5001 Eisenhower Avenue Alexandria, VA 22333
3	Project Manager Tank Main Armament System ATTN: DRCPM-TMA, K. Russell DRCPM-TMA-105 DRCPM-TMA-120 Dover, NJ 07801
3	Commander Armament R&D Ctr, USA AMCCOM ATTN: DRSMC-LCW-A(D) M.Salsbury DRSMC-LCS(D) DRSMC-LC(D)J. Frasier Dover, NJ 07801
5	Commander US Army Armament Munitions and Chemical Command ATTN: DRSAR-LEP-L(R) DRSAR-LC(R), L. Ambrosini DRSAR-IRC(R), G. Cowan DRSAR-LEM(R), W. Fortune R. Zastrow Rock Island, IL 61299
1	Commander US Army Watervliet Arsenal ATTN: SARWV-RD, R. Thierry Watervliet, NY 12189
1	Director US Army AMCCOM Benet Weapons Laboratory ATTN: DRSMC-LCB-TL Watervliet, NY 12189
1	Commander US Army Aviation Research and Development Command ATTN: DRDAV-E 4300 Goodfellow Blvd. St. Louis, MO 63120
3	Commander Armament R&D Center US Army AMCCOM ATTN: DRSMC-TSS(D) DRSMC-TDC(D) DRSMC-OAR(D), J. Rutkowski Dover, NJ 07801

DISTRIBUTION LIST

No. Of Copies	Organization
1	Director US Army Air Mobility Research And Development Laboratory Ames Research Center Moffett Field, CA 94035
1	Commander US Army Communications Research and Development Command ATTN: DRSEL-ATDD Fort Monmouth, NJ 07703
1	Commander US Army Electronics Research and Development Command Technical Support Activity ATTN: DELSD-L Fort Monmouth, NJ 07703
1	Commander US Army Harry Diamond Lab. ATTN: DELHD-TA-L 2800 Powder Mill Road Adelphi, MD 20783
1	Commander US Army Missile Command ATTN: DRSMI-R Redstone Arsenal, AL 35898
1	Commander US Army Natick Research and Development Command ATTN: DRDNA-DT, D. Sieling Natick, MA 01760
1	Commander US Army Tank Automotive Command ATTN: DRSTA-TSL Warren, MI 48090
1	US Army Tank Automotive Command ATTN: DRSTA-CG Warren, MI 48090

No. Of Copies	Organization
1	Project Manager Improved TOW Vehicle ATTN: DRCPM-ITV US Army Tank Automotive Cmd. Warren, MI 48090
1	HQDA (DAMA-ART-M) Washington, DC 20310
2	Program Manager M1 Tank System ATTN: DRCPM-GMC-SA, T. Dean Warren, MI 48090
1	Project Manager Fighting Vehicle Systems ATTN: DRCPM-FVS Warren, MI 48090
1	Director US Army TRADOC Systems Analysis Activity ATTN: ATAA-SL White Sands Missile Range, NM 88002
1	Project Manager M-60 Tank Development ATTN: DRCPM-M60TD Warren, MI 48090
1	Commander US Army Training & Doctrine Command ATTN: ATCD-MA/ MAJ Williams Fort Monroe, VA 23651
2	Commander US Army Materials and Mechanics Research Center ATTN: DRXMR-ATL Tech Library Watertown, MA 02172
1	Commander US Army Development & Employment Agency ATTN: MODE-TED-SAB Fort Lewis, WA 98433

DISTRIBUTION LIST

No. Of Copies	Organization
1	Commander US Army Research Office ATTN: Tech Library P. O. Box 12211 Research Triangle Park, NC 27709
1	Commander US Army Mobility Equipment Research & Development Command ATTN: DRDME-WC Fort Belvoir, VA 22060
1	Commander US Army Logistics Mgmt Ctr Defense Logistics Studies Fort Lee, VA 23801
1	Commandant US Army Infantry School ATTN: ATSH-CD-CSO-OR Fort Benning, GA 31905
1	US Army Armor & Engineer Board ATTN: STEBB-AD-S Fort Knox, KY 40121
1	Commandant US Army Aviation School ATTN: Aviation Agency Fort Rucker, AL 36360
1	Commandant Command and General Staff College Fort Leavenworth, KS 66027
1	Commandant US Army Special Warfare School ATTN: Rev & Tng Lit Div Fort Bragg, NC 28307
1	Commandant US Army Engineer School ATTN: ATSE-CD Ft. Belvoir, VA 22060

No. Of Copies	Organization
1	Commander US Army Foreign Science & Technology Center ATTN: DRXST-MC-3 220 Seventh Street, NE Charlottesville, VA 22901
3	Commandant US Army Armor School ATTN: ATZK-CD-MS/ M. Falkovitch Armor Agency Fort Knox, KY 40121
1	Chief of Naval Materiel Department of the Navy ATTN: J. Amlie Washington, DC 20360
1	Office of Naval Research ATTN: Code 473, R. S. Miller 800 N. Quincy Street Arlington, VA 22217
1	Commander Naval Sea Systems Command ATTN: SEA-62R2, R. Beauregard National Center, Bldg. 2 Room 6E08 Washington, DC 20362
1	Assistant Secretary of the Navy (R, E, and S) ATTN: R. Reichenbach Room 5E787 Pentagon Bldg. Washington, DC 20350
1	Naval Research Lab Tech Library Washington, DC 20375
1	Commander US Army Missile Command ATTN: DRSMI-YDL Redstone Arsenal, AL 35898
1	Commander US Army TSARCOM 4300 Goodfellow Boulevard St. Louis, MO 63120

DISTRIBUTION LIST

No. Of Copies	Organization
5	Commander Naval Surface Weapons Center ATTN: Code G33, J. L. East W. Burrell J. Johndrow Code G23, D. McClure Code DX-21 Tech Lib Dahlgren, VA 22448
2	Commander US Naval Surface Weapons Center ATTN: J. P. Consaga C. Gotzmer Indian Head, MD 20640
4	Commander Naval Surface Weapons Center ATTN: S. Jacobs/Code 240 Code 730 K. Kim/Code R-13 R. Bernecker Silver Spring, MD 20910
2	Superintendent Naval Postgraduate School Dept. of Mechanical Engineering ATTN: A. E. Fuhs Code 1424 Library Monterey, CA 93940
1	AFATL/DLODL ATTN: Tech Lib Eglin AFB, FL 32542
1	AFFDL ATTN: TST-Lib Wright-Patterson AFB, OH 45433
1	AFWL/SUL Kirtland AFB, NM 87117
1	NASA/Lyndon B. Johnson Space Center ATTN: NHS-22, Library Section Houston, TX 77058

Aberdeen Proving Ground

Dir, USAMSAA
ATTN: DRXSY-D
DRXSY-MP, H. Cohen

Cdr, USATECOM
ATTN: DRSTE-TO-F
STEAP-MT, S. Walton
G. Rice
D. Lacey
C. Herud

Dir, HEL
ATTN: J. Weisz

Cdr, CRDC, AMCCOM
ATTN: DRSMC-CLB-PA
DRSMC-ACW
DRSMC-CLN
DRSMC-CLJ-L
DRSMC-CLB-PO (10 cys)

USER EVALUATION SHEET/CHANGE OF ADDRESS

This Laboratory undertakes a continuing effort to improve the quality of the reports it publishes. Your comments/answers to the items/questions below will aid us in our efforts.

1. BRL Report Number_____ Date of Report_____

2. Date Report Received_____

3. Does this report satisfy a need? (Comment on purpose, related project, or other area of interest for which the report will be used.)_____

4. How specifically, is the report being used? (Information source, design data, procedure, source of ideas, etc.)_____

5. Has the information in this report led to any quantitative savings as far as man-hours or dollars saved, operating costs avoided or efficiencies achieved, etc? If so, please elaborate._____

6. General Comments. What do you think should be changed to improve future reports? (Indicate changes to organization, technical content, format, etc.)

CURRENT ADDRESS

Name

Organization

Address

City, State, Zip

7. If indicating a Change of Address or Address Correction, please provide the New or Correct Address in Block 6 above and the Old or Incorrect address below.

OLD ADDRESS

Name

Organization

Address

City, State, Zip

(Remove this sheet along the perforation, fold as indicated, staple or tape closed, and mail.)

FOLD HERE

Director
US Army Ballistic Research Laboratory
ATTN: AMXBR-OD-ST
Aberdeen Proving Ground, MD 21005-5066

NO POSTAGE
NECESSARY
IF MAILED
IN THE
UNITED STATES

OFFICIAL BUSINESS
PENALTY FOR PRIVATE USE, $300

BUSINESS REPLY MAIL
FIRST CLASS PERMIT NO 12062 WASHINGTON, DC
POSTAGE WILL BE PAID BY DEPARTMENT OF THE ARMY

Director
US Army Ballistic Research Laboratory
ATTN: AMXBR-OD-ST
Aberdeen Proving Ground, MD 21005-9989

FOLD HERE